Mon. Not. R. Astron. Soc. **000**, 000–000 (0000) Printed 14 October 2011 (MN LATEX style file v2.2)

Maximal spin and energy conversion efficiency in a symbiotic system of black hole, disk and jet

Zoltán Kovács[1⋆], László Á. Gergely[2,3‡], Peter L. Biermann[4,5,6,7,8†]
[1] *Department of Physics and Center for Theoretical and Computational Physics, The University of Hong Kong, Pok Fu Lam Road, Hong Kong*
[2] *Department of Theoretical Physics, University of Szeged, Tisza Lajos krt. 84-86, Szeged 6720, Hungary*
[3] *Department of Experimental Physics, University of Szeged, 6720 Szeged, Dóm tér 9, Hungary*
[4] *Max-Planck-Institut für Radioastronomie, Auf dem Hügel 69, Bonn, Germany*
[5] *FZ Karlsruhe, and Department of Physics, University of Karlsruhe, Germany*
[6] *Department of Physics and Astronomy, University of Alabama, Tuscaloosa, 35487 AL, USA*
[7] *Department of Physics, University of Alabama at Huntsville, 35899 AL, USA*
[8] *Department of Physics and Astronomy, University of Bonn, Germany*

⋆ *E-mail:zkovacs@hku.hk* ‡ *E-mail:gergely@physx.u-szeged.hu* † *E-mail:plbiermann@mpifr-bonn.mpg.de*

14 October 2011

ABSTRACT

We study a combined model of black hole - accretion disk - magnetosphere - jet symbiosis, applicable for supermassive black holes. We quantify the mass and spin evolution and we analyze how the limiting value of the spin parameter and the conversion efficiency of accreted mass into radiation depend on the interplay of electromagnetic radiation reaction, magnetosphere characteristics and truncation radius of radiation. The dominant effect comes from the closed magnetic field line region, which reduces the spin limit to values $\sim$0.89 (instead $\sim$0.99 in its absence). Therefore observations on black hole spins could favour or disfavour the existence of the closed magnetic field line region (or its coupling to the disk). We also find that the suppression of radiation from the innermost part of the accretion disk, inferred from observations, and a collimated jet both increase the spin limit and the energy conversion efficiency.

1 INTRODUCTION

Ever since it was shown, that almost all galaxies have a central super-massive black hole (Kormendy & Richstone 1995, Faber et al. 1997), it has become of renewed interest to understand the life-cycle of black holes. Is it driven by accretion from an accretion disk (Shakura 1972, Shakura & Sunyaev 1973, Novikov & Thorne 1973), mergers with other black holes (Hughes & Blandford 2003), an alternating sequence of the two (Berti & Volonteri 2008), eating stars whole, spin-down driving a relativistic jet, or some other not yet understood process? Early statistics have already showed that existing black holes are active in the sense to have an accretion disk shine prominently only a small fraction of the time, of order one percent or so.

On the other hand, digging deep with observations in the radio regime shows that even very quiet black holes are all active in the sense of showing compact radio emission. Very long baseline (usually intercontinental) radio interferometry (VLBI) shows that in all cases, when the data are sufficiently deep, the activity is driving a relativistic jet (Chini et al. 1989**,** Nagar et al. 2000, 2001, 2002, 2005, Falcke et al. 2000). This emission is strong, when the jet happens to point in our direction, and so is strongly enhanced by re lativistic boosting. And yet, the power is far sub-Eddington in many such cases. Therefore it is hard to accept that accretion could provide the power. For jets pointing elsewhere these cases populate the low end of the radio luminosity function (Windhorst et al. 1984, 1985, 1990, Perez-Fournon & Biermann 1984). In such cases spin-down almost certainly powers the activity (Blandford 1976).

There are several proposals on the ways of interpreting the compact radio emission, some with emission from the disk itself, and some with emission from a relativistic jet. Since we can directly observe a relativistic jet in some cases, we follow Occam's razor, and adopt the point of view, that all such cases have the same mechanism. Therefore we interpret the compact radio emission as arising from a relativistic jet in all cases (Falcke, Malkan & Biermann 1995; Falcke & Biermann 1995; Falcke 1996; Falcke & Biermann 1996; Falcke & Biermann 1999; Markoff, Falcke & Fender 2001; Yuan, Markoff & Falcke 2002a; Yuan et al. 2002b).

It had been noted early on, that the low radio frequency spectrum suggested a low energy cutoff in the electron energy distribution, such as would naturally occur from the decay of charged pions, created in hadronic collisions (Falcke et al. 1995a, 1995b, 1996, Gopal-Krishna et al. 2004). The site to do this would be the inner accretion disks in a low accretion mode, when the disk turns into a very hot Advection Dominated Accretion Flow (ADAF). For a dimensionless spin-parameter $a_* > 0.95$ the temperature reaches

to relativistic levels (Mahadevan 1998), and the thermal collisions become hadronic, giving rise to pion production. As a consequence such radio spectra suggest that the spin is high. However, in the case, that the jets start purely electrodynamically, as Poynting flux jets, the charged pion production would be in the shocks around stars or compact clouds entering the jets sideways (e.g., Gamma rays from cloud penetration at the base of AGN jets, Araudo et al. (2010)).

As almost all otherwise quiescent super-massive black holes are active in such a sense, it implies that they maintain their spin at a high level, compatible with the suggestion of Blandford (1976), that the decay time of the black hole magnetic fields is very long; this is feasible as long as the power output used to drive the jet is a small fraction of the energy reservoir, the rotation of the black hole. The power output estimated by Whysong & Antonucci (2003) for the radio galaxies M87 (= NGC4486 = Vir A) and NGC5128 (=Cen A) suggests that indeed the power output by the jets is of order $10^{-2.5}$ of the limiting Eddington luminosity, or even less, allowing a long life time. This limit implies that no matter is supplied from the disk to the jet at all, which means that the jet starts as a Poynting flux dominated jet (Sikora et al. 2005). Armitage & Natarajan (1999) confirmed that a fully rotating black hole can power a Poynting flux dominated jet for the very long lifetime of AGNs.

Thus it is of tantamount importance to understand, which process allows the super-massive black holes to attain such a high spin state.

Due to accretion, black holes spin up to the maximal spin limit, even in the absence of initial rotation (Bardeen 1970). For the maximally spinning (extreme) Kerr black holes the efficiency of accreted rest mass conversion into outgoing electromagnetic radiation is 42.3%. A refined accretion model, assuming a geometrically thin, but optically thick steady state accretion disk (composed of rotating plasma with high opacity) was introduced by Shakura & Sunyaev (1973) and Novikov & Thorne (1973). This model takes into account the additional effect of the photons emitted from the disk and captured by the black hole, modifying both the energy and angular momentum transport from the disk into the black hole (Page & Thorne 1974). Therefore the spin evolution and mass growth of black holes is slightly changed as compared to Bardeen's model. The spin limit is reduced to 0.9982 (compared to 1 in the Bardeen approach) for an electron scattering atmosphere; also the conversion efficiency diminishes to 30% (Thorne 1974). The black holes with radiating accretion disks leading to photon capture are referred to as *canonical black holes*, while the accretion disk is discussed in the framework of a *hydrodynamic* model with *steady-state accretion*.

In *magnetohydrodynamic* (MHD) models, magnetic stresses in the disk modify the dynamics of the accretion disk. The study of MHD accretion flows for various magnetosphere models lead to a modified energy and angular momentum transport (Camenzind 1986, 1987, Takahashi et al. 1990, Nitta, Takahashi & Tomimatsu 1991, Hirotani et al. 1992). Blandford & Znajek (1977) have found a mechanism (BZ) of extracting both energy and angular momentum from the rotating black hole via open poloidal magnetic field lines emanating from its event horizon (such that the total magnetic flux over the horizon vanishes). In another configuration of closed poloidal magnetic field lines, also emanating from the event horizon, but anchored in the disk, the energy and angular momentum are exchanged between the rapidly rotating black hole and the slowly rotating disk (Li 2000, Wang, Xiao & Lei 2002).

The BZ mechanism is nowadays regarded as a possible source of powering jets in AGN's and gamma-rray bursts (GRB's), where the angular momentum is carried away by outflowing jets. Jets existing in symbiosis with accretion disks and black holes represent an efficient mechanism for extracting energy and angular momentum from the disk and black hole. Based on Blandford & Königl (1979) arguments, Falcke & Biermann (1996) developed a simple model where the plasma jet emanating from the inner region of the disk forms a *symbiotic* system with the disk and the black hole. This model, in conjunction with the BZ mechanism describes the rest mass, angular momentum and energy transport between the black hole and its environment in the presence of magnetic field and jets. Focusing on the role of jets (by switching off the magnetic field) this symbiotic model was discussed in detail by Donea & Biermann (1996). An alternative model for launching relativistic jets in active galactic nuclei (AGN) from an accreting Kerr black hole by converting the accretion disc energy into jet energy, was recently advanced by Duţan (2010).

Composite models of accretion disks involve a radial transition between a Shakura-Sunyaev disk on the outside to an ADAF on the inside. In an ADAF the heat generated via viscosity is advected inward rather than radiated away. Some composite models apply a geometrically thick and optically thin hot corona (Mannheim et al. 1995) positioned between the marginally stable orbit and the inner edge of the geometrically thin and optically thick accretion disk, lying at a few gravitational radii (Thorne & Price 1975, Shapiro, Lightman & Eardley 1976). In composite models the soft and hard components of the broad band X-ray spectra of galactic black holes were attributed to the thermal radiation of the accretion disk and the emission mechanism in the corona, respectively. In another type of composite models the corona lies above and under the accretion disk and the soft photons arriving from the disk produce a hard emission via their inverse comptonization by the thermally hot electrons in the corona (Liang & Price 1977). In both configurations the soft photon flux of the disk and, in turn, the photon capture effect on the mass-energy growth of the black hole are reduced. The spin evolution and its limiting value are therefore closer to the predictions of Bardeen than for canonical black holes.

We picture the evolution of an activity event of a black hole as follows. Two galaxies interact and feed low angular momentum material into the centers (Toomre & Toomre 1972). In case both have a central black hole, these black holes merge, and typically produce a merged black hole with relatively high spin, of order 0.7 (Berti & Volonteri 2008). Then accretion near maximum levels pushes up the spin to near maximum (Bardeen 1970), and establishes a maximal magnetic field, and a jet, initially weak. When accretion slows down, the jet becomes strong, and the emission from the inner disk dies away. In the following long phase the black hole powers the jet from its rotational energy alone. In the present work we study *the evolution of the spin and mass* of the black hole coexisting in *a symbiotic system with*

a radiatively truncated accretion disk, a pair of jets, and a magnetosphere containing both open and closed field line regions. As no matter is supplied from the disk to the Poynting flux dominated jet, its effect appears only in the suppression of the radiation from the accretion disk in its innermost region. For simplicity, we do not include possible contributions of hard photons radiated away by a hot corona, neither the ADAF mechanism. An ionization instability may also influence the lifetime cycle and overall complexity in the supermassive black hole environment (Janiuk & Czerny 2011). Despite the simplifications, we present the most complete symbiotic model up to date, and we employ it for the study of spin and mass evolution.

In Section 2 we briefly review the elements of the symbiotic model. In Section 3 we discuss the structure equations of the disk, as derived from conservation laws and give a detailed presentation on the effects of the magnetic fields with coexisting open and closed field line topologies. We also discuss the effects on the radial profiles of the flux emitted by the disk and write up a generic flux formula. Section 4 presents study of the evolution of the black hole spin and mass and the modifications induced in the energy conversion efficiency by magnetic fields and jets. Section 5 contains the concluding remarks.

Notation. 4-vectors and tensors are denoted by bold face italic letters. The only exceptions are the Killing vectors $\partial/\partial t$ and $\partial/\partial\phi$. The scalar product of 4-vectors and the contraction of 4-vectors with symmetric tensors are denoted by a dot, i.e., $\boldsymbol{q}\cdot\boldsymbol{u} = q^\mu u_\mu$ and $\boldsymbol{T}\cdot\partial/\partial\phi = T^{\mu\nu}(\partial/\partial\phi)_\mu$, where $T^{\mu\nu} = T^{\nu\mu}$. We use geometrical units, with $G = 1$ and $c = 1$.

2 ELEMENTS OF THE SYMBIOTIC MODEL

In subsection 2.1 we review the dynamics of test particles in the rotating black hole geometry. In subsection 2.2 we summarize the relevant results on accretion disk physics from Shakura & Sunyaev (1973), Novikov & Thorne (1973), Page & Thorne (1974), for later generalization. The presented assumptions regarding geometry and matter stand at the basis of the steady-state, thin accretion disk model. Then in subsection 2.3 we discuss the magnetic field and in subsection 2.4 the characteristics of the jets.

2.1 The geometry

The line element in a stationary, axisymmetric configuration is

$$ds^2 = g_{tt}dt^2 + 2g_{t\phi}dtd\phi + g_{\phi\phi}d\phi^2 + g_{11}d(x^1)^2 + g_{22}d(x^2)^2 \ , \quad (1)$$

with $g_{\mu\nu} \equiv \boldsymbol{g}(\partial/\partial x^\mu, \partial/\partial x^\nu) = (\partial/\partial x^\mu)\cdot(\partial/\partial x^\nu)$ the components of the metric $\boldsymbol{g}$. The coordinates $x^\mu = (t, x^1, x^2, \phi)$ are adapted to the time-like and rotational Killing vector fields $\partial/\partial t$ and $\partial/\partial\phi$. In addition we assume asymptotic flatness and reflection symmetry about the equatorial plane.

Geodesic circular orbits in the equatorial plane are characterized by their angular velocity $\Omega \equiv d\phi/dt$, specific (normalized to mass) energy $\widetilde{E}$ and specific angular momentum $\widetilde{L}$, measured at infinity (Shibata & Sasaki 1998):

$$\Omega = \frac{-g_{t\phi,r} + \sqrt{(g_{t\phi,r})^2 - g_{tt,r}g_{\phi\phi,r}}}{g_{\phi\phi,r}} \ , \quad (2)$$

$$\widetilde{E} = -\boldsymbol{u}\cdot\partial/\partial t = -(g_{tt} + \Omega g_{t\phi})/|\boldsymbol{k}| \ , \quad (3)$$

$$\widetilde{L} = \boldsymbol{u}\cdot\partial/\partial\phi = (g_{t\phi} + \Omega g_{\phi\phi})/|\boldsymbol{k}| \ . \quad (4)$$

Here the 4-velocity $\boldsymbol{u} = \boldsymbol{k}/|\boldsymbol{k}|$ of a stationary observer is determined by

$$\boldsymbol{k} = \partial/\partial t + \Omega\partial/\partial\phi \ , \quad (5)$$

with norm

$$|\boldsymbol{k}| = \sqrt{-g_{tt} - \Omega g_{t\phi} - \Omega^2 g_{\phi\phi}} \ . \quad (6)$$

As Ω does not depend on either t or ϕ, it is a constant on the transitivity surfaces of the two Killing vectors and therefore $\boldsymbol{k}$ is also a Killing vector.

The back-reaction of orbiting particles to the geometry (1) is neglected, considering effectively a vacuum. The vacuum space-time obeying axial symmetry, stationarity and asymptotic flatness is the Kerr space-time, characterized by two constants, its mass M and angular momentum J, given by

$$ds^2 = -\frac{\Sigma\Delta}{A}dt^2 + \widetilde{\omega}^2(d\phi - \omega dt)^2 + \frac{\Sigma}{\Delta}dr^2 + \Sigma d\theta^2 \ , \quad (7)$$

with the metric functions

$$\Sigma = r^2 + a^2\cos^2\theta \ , \quad (8)$$

$$\Delta = r^2 + a^2 - 2Mr \ , \quad (9)$$

$$A = (r^2 + a^2)^2 - a^2\Delta\sin^2\theta \ , \quad (10)$$

$$\widetilde{\omega}^2 = A\sin^2\theta/\Sigma \ . \quad (11)$$

The Kerr black hole has two horizons (the roots of $\Delta = 0$) at $r_\pm = M(1 \pm \sqrt{1 - a_*^2})$, where $a = J/M$ and $a_* = a/M = J/M^2$ are the dimensional and dimensionless spin parameters, respectively.

In the vicinity of the equatorial plane the coordinate $z = r\cos\theta$ is suitable to replace θ such that the Kerr metric is approximated as

$$ds^2 = -\mathscr{D}\mathscr{A}^{-1}dt^2 + r^2\mathscr{A}(d\phi - \omega dt)^2 + \mathscr{D}^{-1}dr^2 + dz^2 \ . \quad (12)$$

Eqs. (2)-(4) then become

$$\Omega = M^{-1}x^{-3}\mathscr{B}^{-1} \ , \quad (13)$$

$$\widetilde{E} = \mathscr{C}^{-1/2}\mathscr{G} \ , \quad (14)$$

$$\widetilde{L} = Mx\mathscr{C}^{-1/2}\mathscr{F} \ , \quad (15)$$

with

$$\mathscr{A} = 1 + a_*^2x^{-4} + 2a_*^2x^{-6} \ , \quad (16)$$

$$\mathscr{B} = \pm(1 \pm a_*x^{-3}) \ , \quad (17)$$

$$\mathscr{C} = 1 - 3x^{-2} \pm 2a_*x^{-3} \ , \quad (18)$$

$$\mathscr{D} = 1 - 2x^{-2} + a_*^2x^{-4} \ , \quad (19)$$

$$\mathscr{G} = 1 - 2x^{-2} \pm a_*x^{-3} \ , \quad (20)$$

$$\mathscr{F} = \pm(1 \mp 2a_*x^{-3} + a_*^2x^{-4}) \quad (21)$$

and

$$\omega = 2M^{-1}a_*x^{-6}\mathscr{A}^{-1} \ . \quad (22)$$

Here $x = \sqrt{r/M}$ (Novikov & Thorne, Page & Thorne 1974).

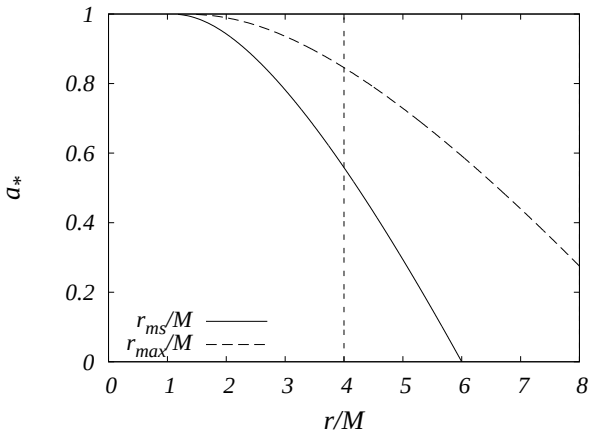

Figure 1. The relation between the spin parameter a_* and the marginally stable orbit r_{ms} (solid curve), as given by Eq. (23). At $r = 4M$ (vertical dashed line) the radiative truncation is possible only for fairly rapidly rotating black holes with $0.56 \leqslant a_* \leqslant 1$. For $r > 6M$ the radiative truncation is possible at any a_*. The dashed curve shows for each a_* the value of the radius, where the flux F emitted by the accretion disk is maximal, obtained by extremizing Eq. (50) with respect to r/M.

In Eqs. (16)-(21) the upper (lower) signs refer to corotating (retrograde) orbits.[1]

A particle with zero orbital angular velocity falling into the Kerr black hole will be subject to the frame dragging effect, and as a result will acquire an angular velocity $\Omega^H \equiv \Omega\left(r_+\right) = a_*/2r_+$, known as the horizon rotational velocity.[2]

The innermost marginally stable circular geodesic orbit, with coordinate radius r_{ms} is given by (Bardeen, Press & Teukolsky 1972), which rewritten in the dimensionless variable $x_{ms} = \sqrt{r_{ms}/M}$ reads:

$$x_{ms}^4 - 6x_{ms}^2 \pm 8a_* x_{ms} - 3a_*^2 = 0 \ . \tag{23}$$

Special solutions include the Schwarzschild limit $a_* = 0$, in which we recover $r_{ms} = 6M$; and the extreme Kerr limit $a_* = 1$ for which we get $r_{ms} = M$ for corotating and $r_{ms} = 9M$ for counterrotating particles. The generic dependence of r_{ms} on a_* is represented on Fig. 1.

2.2 The accretion disk

Particles on circular geodesic orbits in the equatorial plane of the black hole form an accretion disk of plasma. Novikov & Thorne (1973) have introduced the hydrodynamic model of an anisotropic fluid for the disk with the energy-momentum tensor

$$\boldsymbol{T}^{HD} = \rho_0 \boldsymbol{u} \otimes \boldsymbol{u} + \boldsymbol{u} \otimes \boldsymbol{q} + \boldsymbol{q} \otimes \boldsymbol{u} + \boldsymbol{t} \ . \tag{24}$$

Here $\boldsymbol{u}$ is the 4-velocity, ρ_0 the density, $\boldsymbol{q}$ the energy flow vector and $\boldsymbol{t}$ the stress tensor in the averaged rest-frame, obeying $\boldsymbol{u} \cdot \boldsymbol{q} = 0 = \boldsymbol{u} \cdot \boldsymbol{t}$. The matter variables ρ_0, $\boldsymbol{q}$ and $\boldsymbol{t}$ are local, unaveraged quantities. A generalization of the above energy-momentum tensor would be to add the specific internal energy $\Pi \boldsymbol{u} \otimes \boldsymbol{u}$, however Page & Thorne (1974) justifiably assume that this is negligible compared to the gravitational potential energy.

Due to the axial and stationary symmetry of the geometry it is practical to introduce averages over ϕ and t for any (tensorial) matter quantity Ψ as

$$\langle \Psi(z,r) \rangle = \frac{1}{2\pi\Delta t} \int_t^{t+\Delta t} \int_0^{2\pi} \Psi(t,r,z,\phi) dt d\phi \ , \tag{25}$$

where Ψ is Lie dragged along $\partial/\partial t$ and $\partial/\partial\phi$ and Δt is a characteristic time scale.

The maximum half thickness H_{disk} of the disk being much less, than its characteristic radial scale, the disk is considered geometrically thin. Optically however, the disk is thick, thus it has high opacity. Its surface energy density is

$$\Sigma_{disk}\left(r\right) = \int_{-H_{disk}}^{H_{disk}} \langle \rho_0 \rangle \, dz \ , \tag{26}$$

where

$$u^r_{disk} = \Sigma^{-1}_{disk} \int_{-H_{disk}}^{H_{disk}} \langle \rho_0 u^r \rangle \, dz \tag{27}$$

represents the radial velocity of the local rest frame of the baryons. Then the radial rest mass flow through the ring is defined as

$$\dot{M}_0 = -2\pi r \Sigma_{disk} u^r_{disk} \tag{28}$$

(the minus sign arises from the fact that u^r_{disk} point outwards, while the mass flow is inwards).

Following Page & Thorne 1974 we assume that there is no energy flow in the disk ($q^r = 0 = q^\phi$), therefore any energy flow is entirely in the z-direction. We also define the average of the energy flow vector $\boldsymbol{q}$ as

$$F = \langle q^z(H_{disk}) \rangle = -\langle q^z(-H_{disk}) \rangle \ , \tag{29}$$

(the last equality coming from the reflection symmetry over the equatorial plane, thus F will have opposed signs if evaluated at the upper or lower disk boundary) and ${W_\phi}^r$ as the $r\phi$-component of the averaged stress tensor $\boldsymbol{t}$, integrated over the thickness of the disk

$${W_\phi}^r = \int_{-H_{disk}}^{H_{disk}} \left\langle {t_\phi}^r \right\rangle dz \ . \tag{30}$$

This hydrodynamic model is useful as long as the effect of the magnetic fields on the geometry and null geodesics is at most of the order of the Larmor radius (small compared to the gravitational radius).

2.3 The magnetic field

The thin disk models can be generalized by considering external magnetic fields around the accretion disk - black hole system. The topology of the black hole magnetosphere consists of open and closed flux lines. Open flux lines emanate from the event horizon or the disk and extend to infinity forming a jet, whereas closed ones connect the horizon and the accretion disk (Macdonald & Thorne 1982). Open field lines also could emanate from the outer disk region, outside the maximal extension of the closed line region (Uzdensky 2005).

[1] In SI units distances are conveniently expressed in units of GM/c^2 (the gravitational radius). In our chosen units then distances can be expressed in units of M.

[2] All indices ^{H} refer to the outer horizon of the Kerr black hole.

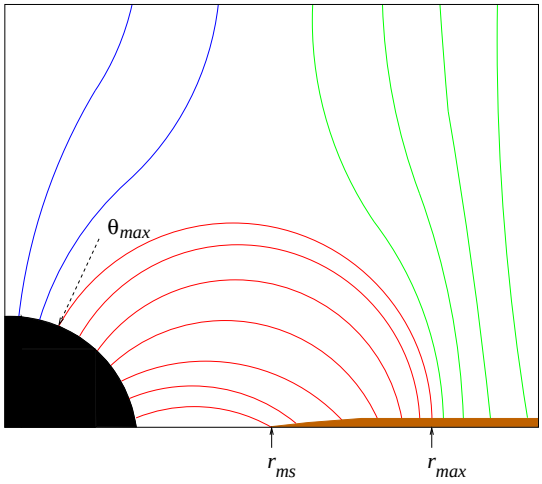

Figure 2. The open and closed magnetic field line topology.

The magnetic field geometry in accretion flows in the relativistic case was studied by many, especially by Hirose et al. (2004) and McKinney (2005), building on earlier work. Our approximation constitutes a subset of their configurations, and one of their results is that the configuration connecting black hole and disk is more important for thin disks and does not transfer significant amounts of angular momentum. However, since we argue for a radiative inner edge of the accretion disk to be possibly far outside the inner-most stable orbit, a direct comparison is difficult.

The open field line topology emanating from the horizon provides the basic idea for the Blandford-Znajek (BZ) mechanism, which describes how rotational energy and angular momentum can be extracted electromagnetically from the spinning hole and transported to large distances in the form of a Poynting flux jet (Blandford & Znajek, Znajek 1977, Hirose et al. 2004, McKinney 2005). Let Ω^F denote the rotational velocity of the open magnetic field lines. We assume the maximally efficient BZ mechanism, which implies that at the event horizon $\Omega^F(r_H) = \Omega^H/2$.

The magnetic field at the horizon is given by the history of accretion to the black hole (Blandford & Znajek 1977). The strength of magnetic field at the horizon can be written in the term of the accretion rate of the rest mass (Moderski & Sikora 1996) as

$$B_H^2 = \frac{2\dot{M}_0}{r_H^2} \ . \tag{31}$$

We assume Eq. (31) to hold in our model. This approximation was also found in considerations by Krolik (1999) to be generally valid.

In addition to the parameters B_H and Ω^F of the open magnetic field, we introduce the opening angle θ_{max} of the cone separating open and closed field lines in each hemisphere. The open magnetic field lines emanate from the horizon for $0 < \theta < \theta_{max}$, whereas the closed ones connect the horizon to the disk between θ_{max} and the equatorial plane. The maximal extension of the closed magnetic field on the disk is at $r_{\rm max}$, outside which another open field line system begins. We sketch this configuration on Fig. 2.

For the closed magnetic field, Wang, Xiao & Lei (2002) employed the power law distribution $B_D \propto r^{-n}$, $0 < n < 3$ given by Blandford (1976) and defined the poloidal component B_D on the disk as

$$\frac{B_D}{B_H} = \frac{r_H}{\widetilde{\omega}(r_{ms})} \left(\frac{r}{r_{ms}}\right)^{-n} \ . \tag{32}$$

They assumed that the pressures due to the magnetic field and infalling matter are in balance at the inner edge of the disk (r_{ms}) and the ratio B_H/B_D varies from 1.8 to 3 for $0 < a_* < 1$.

As the closed field lines connect the event horizon to the accretion disk, the rotating black hole exerts a magnetic torque on the disk, provided the flux lines are frozen into the plasma (ideal MHD condition). This torque transfers angular momentum and energy from the black hole to the disk ($\Omega < \Omega^H$ is assumed), modifying the global energy and angular momentum balance (Li 2000, 2003).

In the MHD simulations of Hirose et al. (2004) these magnetic field configurations were found to be uncommon, connecting the black hole horizon to the disk. However, since we include a radiative cutoff of the inner disk, inspired by observations, our configuration is not readily compared to theirs. Also, we have the additional free parameter of a maximum latitude θ_{max} of magnetic field lines connecting, which allows the black hole to be stronger or weaker in its effect on the jet than given by the current accretion rate as considered in Hirose et al. (2004). Simulations of such configurations would be very useful, when the black hole has acquired already its maximal magnetic field, and then the accretion rate dips below its earlier rate; then the newly accreted field is weaker, and the separatrix between disk connection and jet configuration could be different, resulting in a different θ_{max}.

By solving numerically the Grad-Shafranov (GS) equation, Uzdensky (2005) studied the topology of a stationary axisymmetric force-free degenerate magnetosphere of a Kerr black hole with closed field lines between the event horizon and a thin, Keplerian, infinitely conducting accretion disk. He assumed the radius $r_{\rm max}$ proportional to ψ_H/ψ_D, the ratio of the total flux measured at the event horizon and on the disk at $r_{\rm max}$ (his Eq. (42), plausible, but labelled by him as arbitrary). This is a modified counterpart of the Blandford power law given by Eq. (32), with qualitative agreement for the power $n = 3$ (modulo a scaling factor).

The Uzdensky (2005) solution of the GS equation determines the radial extension of the field lines anchored in the disk as a function of the spin. In the limit of slow rotation the size of the magnetically connected inner part of the disk decreases with the increasing black hole spin. We stress here that the model we adapt (based on the Blandford power law) also predicts this shrinking of the closed magnetic field region with increasing spin, as illustrated on Fig. 3.

Uzdensky did not include any magnetic field lines running from the black hole to infinity, and so in our language his $\theta_{max} = 0$. Our model includes the jet, and hence the open magnetic field lines emanating from the horizon, thus θ_{max} is a free parameter. Uzdensky solves a different problem, the one for a jet-less black hole, and so it is not immediately obvious how to directly use his results for the more general setup we discuss. Therefore the application of the Blandford power law for the ratio B^H/B^D seems to us to be the most straightforward way to compare the effect of the truncation of the radiation on the spin evolution with previous results.

2.4 The jet

Numerical simulations of rotating black holes with a magnetosphere and a thin accretion disk produced realistic jet profiles which have a complicated double layer structure with an inner gas pressure-driven and an outer magnetically driven jet (Mizuno et al. 2006). For the magnetically driven jets the open field lines may be connected to the disk, without touching the event horizon. These magnetohydrodynamic mechanisms dissipate energy and pump angular momentum from the disk into the jet. The black hole spin evolution is driven by spin-down to drive the jet and independently by spin-up by accretion from the disk.

With a non-zero 4-velocity component u^{ϕ}, the plasma forms a jet extracting rest mass, angular momentum and energy from the disk. The loss of matter by the jets is specified by the parameter

$$q_{jet} = \frac{\dot{M}_{jet}}{\dot{M}_0} \in [0, 1) \, , \tag{33}$$

where $0 \leqslant q_{jet} < 1$ (vanishing in our model) and $\dot{M}_{jet}$ is the rate of the rest mass flow into the jet (Falcke & Biermann 1995). As the geometry is reflection symmetric with respect to the equatorial plane, $\dot{M}_{jet}$ is composed of two equal contributions, of the upstream and downstream jets.

The balance equations for mass, angular momentum and energy in the presence of the jets were derived in Donea & Biermann (1996), with parameters q_{jet} and r_{in} (the cut-off radius of the radiating disk) describing the global properties of the jet.

We adopt the simplified approach as in Falcke & Biermann (1995). The differential rotation of the orbiting plasma winds up the radial magnetic field lines acting as a dynamo which generates a poloidal magnetic field. The latter produces a vertical Poynting flux jet, containing negligible baryonic matter. The jet being in a Poynting flux limit implies $q_{jet} = 0$. This assumption decouples the energy and angular momentum transport in the jet from the accretion disk properties.

Almost all supermassive black holes show signs of relativistic jets (Perez-Fournon & Biermann 1984, Chini et al. 1989, Falcke et al. 2000**,** Nagar et al. 2000, 2001, 2002, 2005), exhibiting compact radio emission and extreme variability in this emission (the explanation of this variability needing relativistic motion). The jet activity is correlated with the high spin. Should this really be true for the vast majority of otherwise quiescent black holes, this would be consistent with the hypothesis, that these black holes are in a high spin state. Theoretical estimates are consistent with assuming that the intrinsic Poynting flux of a black hole in a high spin state is of order of $10^{-2.5}$ of the Eddington luminosity (Armitage & Natarian 1999), also consistent with the data on some nearby radio galaxies, Cyg A, M87 and Cen A (Whysong & Antonucci 2003). This low value implies that the lifetime of activity in this state is about the Hubble time. In other worlds the spin-down due to the jet is inefficient, the jet driving can be maintained for extremely long times, independently of any accretion. This low backreaction is the main reason we will not include the jet contribution in the balance equations.

2.5 The inner disk

There is observational evidence from the source GRS1915+105 (Fender et al. 2003, Eikenberry 1998) that the innermost region of the disk does not radiate when the jet is strong. We will therefore assume that unless in the exterior luminous part of the disk, where energy is dissipated, below a certain radius r_{in} the disk does not radiate. Thus all energy and angular momentum from this region is transported into the black hole, hence powering up the jet. The jet is not connected to the disk directly, but only to the black hole, allowing it to start as a pure Poynting flux. Baryonic matter is added into the jet only later, far up from the black hole by intersecting clouds, stars, stellar winds and from shear and boundary instabilities (Araudo et al. 2010). This model allows the early Lorentz factor of the jet flow to be very high, as recently suggested by various observations (see e.g. Ghisellini & Tavecchio 2008).

In Abramowicz et al. (1978) the equipotential surfaces in the absence of magnetic fields were employed to derive the thickness of the disk near the inner edge. It was shown that a non-radiating disk can no longer be described as geometrically thin, its pressure becomes important for the radial disk structure, and the inner edge is pushed in the region between the marginally stable and the marginally bound circular orbits. For Schwarzschild black hole the marginally stable orbit is at $6M$, while the innermost bound circular orbit is at $4M$. With increasing black hole spin the marginally stable orbit approaches the horizon, the marginally bound orbit being trapped in between, their difference becoming very small.

We also argue that all angular momentum of the accretion disk goes into the black hole from the interior zone, independent of whether the disk is thick or thin, either by direct accretion or via the torques of the closed magnetic field lines and the details of this transfer do not matter in a quasi-stationary situation. In particular, the exact location of the exact inner edge of the disk (below r_{in}) does not influence the angular momentum transport towards the black hole; all goes in. These considerations enable us to use as a good approximation for the inner edge of the disk the marginally stable orbit, especially at the high spin values investigated in this paper.

What we have then is a radiatively truncated thin disk, with the inner edge of the radiation zone at r_{in} (instead of r_{ms} in the absence of the jet). The truncated disk model may also be consistent with the composite (ADAF) models where the inner edge of the thin disk under a hot corona can be found at a radius estimated between $2M$ and $100M$ (Done, Madejski & Życki, 2000). For our analysis we chose radiative truncation radii between $4M$ and $12M$ which is twice the range of radii considered by Donea & Biermann (1996). With this larger range the radiative truncation effect on the mass accretion becomes easier to study. Fig. 1 shows the radius of the marginally stable orbit as function of the spin parameter, as given by Novikov & Thorne (1973) and Page & Thorne (1974).

This approximation is different from what was considered by Gammie (1999), Krolik (1999); and Agol & Krolik (2000), all of whom considered the conditions at the innermost stable orbit. Our work is complementary to theirs, but as noted earlier supported by observations of the source

GRS1915+105 as useful to consider (see also Donea & Biermann (1996)).

For lower values of the spin parameter, $a_* \approx 0.56$; the inner edge of the thin disk is located at higher radii than $4M$, so the truncation of the radiation at $4M$ is not possible. The radiative truncation at any radius greater than $6M$ is however possible for the whole range of the spin parameter.

3 STRUCTURE EQUATIONS OF THE DISK

For standard accretion disks Page & Thorne (1974) derived the integral form of the conservation laws of rest mass M_0, angular momentum and energy of the the accretion disk and black hole. The global transport equations were obtained by averaging the continuity equation and the total divergence of the density-flux 4-vectors of total angular momentum $\boldsymbol{J} = \boldsymbol{T} \cdot \partial/\partial\phi$ and energy $\boldsymbol{E} = -\boldsymbol{T} \cdot \partial/\partial t$, respectively.

In subsection 3.1 we generalize this result by including the effects of the magnetic field lines. We discuss the various source terms appearing in the balance equations in the remaining subsections, also the power and torque of the open magnetic field lines.

3.1 Balance equations in the symbiotic model

3.1.1 Rest mass conservation

Rest mass conservation implies that the time averaged rate of the accretion of rest mass (the radial matter flow through a ring of thickness Δr), given by Eq. (28) is independent of the radius (Page & Thorne 1974)

$$\dot{M}_0 = -2\pi r \Sigma_{disk} u^r_{disk} = const. \tag{34}$$

for any $r > r_{in}$.

3.1.2 Angular-momentum conservation

The angular momentum balance equation is found by repeating the derivation (22)-(27) of Page & Thorne (1974), and adding the magnetic contribution. It is necessary to use $(-g)^{1/2} = r$ emerging from Eq. (12), that $u_\phi = \widetilde{L}$, employ the time and azimuthal averaging and the reflection symmetry about the plane $z = 0$ (such that $u^z_{jet}(-z) = -u^z_{jet}(z)$). The angular momentum transport equation becomes

$$[\dot{M}_0 \widetilde{L} - 2\pi r W_\phi{}^r]_{,r} = 4\pi r F \widetilde{L} - \left(\frac{d\Delta L^D}{dt}\right)_{,r} . \tag{35}$$

The torque $d\Delta L^D/dt$ exerted on the disk by the spinning black hole via the closed magnetic field lines gives an additional term, which will be calculated in subsection 3.3.

Eq. (35) represents the balance of four types of contributions determining the angular momentum transport from the disk to the black hole. On the left hand side there are the contributions of the rest mass flow $\dot{M}_0$ and the torques in the disk, on the right hand side the contributions of the flux F of the radiation emitted from the surface of the disk and the contribution of the closed magnetic field lines.

3.1.3 Energy conservation

Energy conservation arises from the balance of the energy transport in terms of the rest mass accretion, torques in the disk (left hand side terms) and the surface radiation and contribution of the closed magnetic field (right hand side terms). Similar considerations as for the rest mass and angular momentum conservations lead to

$$[\dot{M}_0 \widetilde{E} - 2\pi r \Omega W^r{}_\phi]_{,r} = 4\pi r F \widetilde{E} - P^D_{,r} . \tag{36}$$

The expression of the extracted power P^D will be given in subsection 3.3. Again, only the closed field lines contribute.

The expressions (36) and (35) are the *radial structure equations* of the accretion disk with external magnetic fields and jets.

3.2 Power and torque on open magnetic field lines

Although not contributing to the structure equations of the disk, we present here the energy and angular momentum transport due to the BZ mechanism, as they will contribute to the mass and spin evolution of the black hole, to be discussed in Section 4. These transport phenomena have been described in the framework of a 3+1 decomposition of the Kerr geometry (Macdonald & Thorne 1982, Thorne, Price & Macdonald 1986). In the 3+1 formalism the torque exerted on the open magnetic field lines by the rotating black hole can be expressed as an the integral across a surface $\mathscr{S}$ intersecting all open field lines emanating from the horizon and $d\psi$ represents an element of the flux tube ψ transverse to $\mathscr{S}$.

$$-\frac{d\Delta L^H}{dt} = \int_{\mathscr{S}} \frac{\Omega^H - \Omega^F}{4\pi} \widetilde{\omega}^2 B_H d\psi , \tag{37}$$

The power transmitted by this torque and pumped into the flux tube becomes

$$P^H = \int_{\mathscr{S}} \Omega^F \frac{\Omega^H - \Omega^F}{4\pi} \widetilde{\omega}^2 B_H d\psi , \tag{38}$$

where $\widetilde{\omega}$ is the cylindrical radius of flux tube at the event horizon, given by Eq. (11), and B_H is the strength (31) of the magnetic field normal to the horizon.

In order to determine these quantities in the BZ process, we integrate over the open field lines spanning between $\theta = 0$ and θ_{max}, in both hemispheres. Evaluating the integrands in Eqs. (37) and (38) on the horizon and expressing the magnetic flux ψ as a function of θ, we obtain the net torque and the extracted power due to the BZ process as

$$-\frac{d\Delta L^H}{dt} = 8M^3 B_H^2 \int_0^{\theta_{max}} \frac{(\Omega^H - \Omega^F) r_+^2 \sin^3\theta}{2M - r_- \sin^2\theta} d\theta \tag{39}$$

and

$$P^H = 8M^3 B_H^2 \int_0^{\theta_{max}} \frac{\Omega^F (\Omega^H - \Omega^F) r_+^2 \sin^3\theta}{2M - r_- \sin^2\theta} d\theta . \tag{40}$$

In the particular case of $\theta_{max} = \pi/4$ Eqs. (39) and (40) give values close to those of the prevalent approximations (e.g. Park & Vishniac 1988 and Moderski & Sikora 1996)

$$-\frac{d\Delta L^H}{dt} \simeq \frac{1}{8} B_H^2 r_H^4 (\Omega^H - \Omega^F) , \tag{41}$$

$$P^H \simeq \frac{1}{8} B_H^2 r_H^4 \Omega^F (\Omega^H - \Omega^F) \tag{42}$$

for rapidly rotating black holes with $a_* \simeq 0.98$. Since we assumed the rotation frequency $\Omega^F = \Omega^H/2$ at the event horizon (maximally efficient BZ mechanism), Eqs. (39) and (40) can be integrated analytically. For $a_* > 0$ the result is

$$-\frac{d\Delta L^H}{dt} = 8M^3 B_H^2 (\Omega^H - \Omega^F)\frac{r_+^2}{r_-}\left[\cos\theta_{max} - 1 - \frac{2}{a_*}\tan^{-1}\left(\frac{r_-}{Ma_*}\cos\theta_{max}\right) + \frac{2}{a_*}\tan^{-1}\left(\frac{r_-}{Ma_*}\right)\right] \quad (43)$$

and

$$P^H = -\Omega^F d\Delta L^H/dt\,. \quad (44)$$

3.3 Power and torque on closed magnetic field lines

The effects of the closed magnetic field lines on the disk arise in a similar fashion. The torque and the power emerging from the magnetic coupling between the black hole and the disk was derived by Wang, Xiao & Lei (2002), applying the model developed by Li (2000). The torque is:

$$-\frac{d\Delta L^D}{dt} = \int_{\mathscr{S}}\left(\frac{\Omega^H - \Omega}{4\pi^2}\right)\frac{d\psi}{dZ^H}d\psi\,, \quad (45)$$

where dZ^H is the total impedance of the event horizon over the surface $\mathscr{S}$ threaded by all closed field lines. Similarly, the power transferred by the magnetic torque can be written as

$$P^D = \int_{\mathscr{S}}\Omega\left(\frac{\Omega^H - \Omega}{4\pi^2}\right)\frac{d\psi}{dZ^H}d\psi\,. \quad (46)$$

Employing the flux conservation in an arbitrary flux tube between the horizon and the disk, the integrals from Eqs. (45) and (46) can be rewritten as integrals over the radial coordinate. By virtue of Eq. (32), the equations (45) and (46) lead to (Wang et al. 2003):

$$-\frac{d\Delta L^D}{dt} = \frac{4M^2B_H^2}{\sqrt{\mathscr{A}(x_{ms})}}\int_{r_{ms}}^{r_{max}}(\Omega^H - \Omega)\left(\frac{r}{r_{ms}}\right)^{1-n} \times\sqrt{\frac{\mathscr{A}}{\mathscr{D}}}\frac{r_+^2\sin^2\theta}{2M - r_-\sin^2\theta}dr \quad (47)$$

and

$$P^D = \frac{4M^2B_H^2}{\sqrt{\mathscr{A}(x_{ms})}}\int_{r_{ms}}^{r_{max}}\Omega(\Omega^H - \Omega)\left(\frac{r}{r_{ms}}\right)^{1-n} \times\sqrt{\frac{\mathscr{A}}{\mathscr{D}}}\frac{r_+^2\sin^2\theta}{2M - r_-\sin^2\theta}dr\,, \quad (48)$$

where

$$\sin^2\theta = 1 - \left[\frac{1}{2M\sqrt{\mathscr{A}(x_{ms})}}\int_{r_{ms}}^{r}\left(\frac{r}{r_{ms}}\right)^{1-n}\sqrt{\frac{\mathscr{A}}{\mathscr{D}}}dr\right]^2. \quad (49)$$

The radial coordinate r_{max} of the outermost closed flux line emanating from the horizon at the angle θ_{max} can be determined by substituting θ_{max} in Eq. (49). In the prefactor of the integrals the function $\mathscr{A}$ is evaluated at the marginally stable orbit x_{ms}. These expressions are sources in the global angular momentum and energy balance equations. Fig. 3

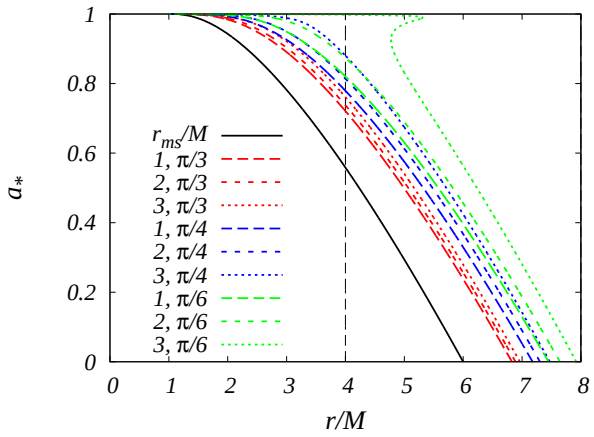

Figure 3. The spin parameter a_* as function of the maximal radius r_{max} (representing the maximal extension of the closed magnetic field lines emanating from the horizon), for various parameter values $n = 1$, 2, 3 and $\theta_{max} = \pi/3$, $\pi/4$, $\pi/6$. The solid (black) curve indicates the value of r_{ms} for each a_* (representing the minimal extension of the closed magnetic field lines). The radius $4M$ (the minimal radiative truncation radius) is indicated by the vertical dashed line.

shows the radii r_{ms} and r_{max} for the power law exponent $n = 1$, 2 and 3 and the boundary angle $\theta_{max} = \pi/3$, $\pi/4$ and $\pi/6$ in the full range of the spin parameter. The closed flux lines connect the event horizon to the disk, ending at radial coordinates contained between r_{ms} and r_{max} for each configuration of a_*, n and θ_{max}. When the radiation from the innermost part of the disk is suppressed, r_{ms} has to be replaced with r_{in}. The closed magnetic field line configuration is determined by Eq. (49). We illustrate this for both the Schwarzschild black hole and a high spin $a_* = 0.99$ black hole on Fig. 4. For each value of the polar angle θ under which the open lines emanate from the horizon there is a well-defined radius r where they couple to the disk. We recover that $r_{\rm max}$ is decreasing with increasing spin, a property also shown by Uzdensky (2005).

3.4 The flux of the radiation emitted from the disk

3.4.1 Standard accretion disk

By eliminating the torque term from the conservation laws, then employing the energy-angular momentum relation $\widetilde{E}_{,r} = \Omega\widetilde{L}_{,r}$ for circular geodesic orbits, Page & Thorne (1974) obtained the radial distribution of the time-averaged radiation emitted from the surface of standard accretion disk as

$$F(r) = -\frac{\dot{M}_0}{4\pi r}\frac{\Omega_{,r}}{(\widetilde{E} - \Omega\widetilde{L})^2}\int_{r_{ms}}^{r}(\widetilde{E} - \Omega\widetilde{L})\widetilde{L}_{,r}dr\,. \quad (50)$$

Since the inner edge of the disk is located at the marginally stable orbit r_{ms} they set the lover boundary of the flux integral to this radius. They also prescribed the *no-torque inner boundary condition* at r_{ms} (which sets the integration constant to zero), by arguing that accreting matter at the marginally stable orbit falls freely into the black hole, unable to exert considerable torque on the disk. The explicit

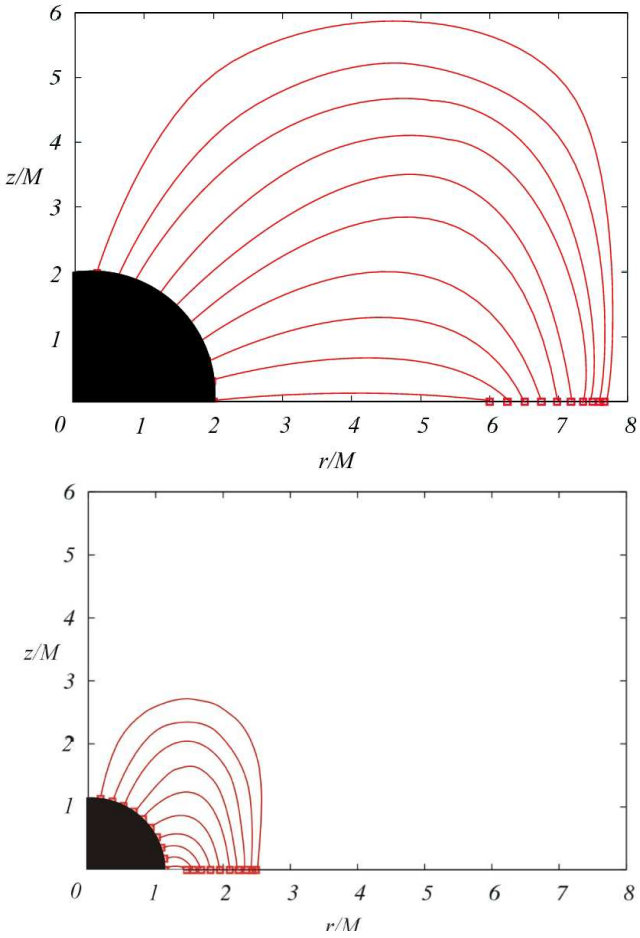

Figure 4. The closed magnetic field configuration for the Schwarzschild black hole (upper sketch) and a rapidly rotating, $a_* = 0.99$ black hole (lower sketch). The endpoints of the magnetic field lines were determined by Eq. (49) for $n = 1$.

analytic expression of F is given as Eq. (A3) of Appendix A. Remarkably, with $r = Mx^2$ the flux F becomes manifestly proportional to $\dot{M}_0/M^2$, the proportionality factor depending only on a_* and x.

Although the no-torque inner boundary condition might not hold if closed magnetic field lines connecting the inner edge of the disk and the event horizon convey torque from the hole to the disk (Krolik 1999, Gammie 1999, Agol & Krolik 2000), Afshordi and Paczyński (2003) have proven that the torque at the inner edge can be neglected in the *absence* of *large scale* radial magnetic fields in the plunging region. In another analytic model developed by Li (2003) the magnetic field lines connect the surface of the disk to higher latitudes of the event horizon. As a consequence, the torque is transported outwards in the disk and it vanishes at the inner edge. Following this model in our symbiotic scheme the magnetic field will not produce considerable effects in the *plunging* region and we can also impose the no-torque boundary condition.

3.4.2 Symbiotic model

The torque term from Eqs. (35) and (36) can be eliminated in the generic case either. By integrating the result, the flux of the disk is obtained as:

$$F_{tot} = F + \frac{\dot{M}_0}{4\pi r}\frac{\Omega_{,r}}{(\widetilde{E}-\Omega\widetilde{L})^2}\int_{r_{in}}^{r}(\widetilde{E}-\Omega\widetilde{L}) \times\left[c_L-\left(\frac{c_E-\Omega c_L}{\Omega_{,r}}\right)_{,r}\right]dr\ . \quad (51)$$

with

$$c_L \equiv -\dot{M}_0^{-1}(d\Delta L^D/dt)_{,r}\ , \quad (52)$$

$$c_E \equiv -\dot{M}_0^{-1}P^D_{,r}\ . \quad (53)$$

Here F is given in Eq. (50), with the modification that its lower integration limit should be r_{in}, rather than r_{ms} (provided $r_{in} > r_{ms}$, otherwise r_{ms}). Integrating by parts the second term on the right hand side of Eq. (51) we obtain

$$F_{tot} = F + \frac{\dot{M}_0}{4\pi r}\frac{\Omega_{,r}}{(\widetilde{E}-\Omega\widetilde{L})^2}\left\{\left[\frac{(\widetilde{E}-\Omega\widetilde{L})}{-\Omega_{,r}}(c_E-\Omega c_L)\right]_{r_{in}}^{r} + \frac{\dot{M}_0}{4\pi r}\int_{r_{in}}^{r}\frac{(\widetilde{E}-\Omega\widetilde{L})}{\Omega}[hc_E+(1-h)\Omega c_L]dr\right\}\ . \quad (54)$$

Here we introduced the shorthand notation

$$h(x,a_*) \equiv \frac{[\ln(\widetilde{E}-\Omega\widetilde{L})]_{,r}}{[\ln\Omega]_{,r}} = -\frac{\mathscr{F}}{x^2\mathscr{C}}$$

with the functions $\mathscr{C}$ and $\mathscr{F}$ given by Eqs. (18) and (21).

The photon flux F_{tot} emitted by the accretion disk depends on the parameters introduced in the global description of the unified model. For a given rotation frequency Ω^F of the magnetic field, the topology of magnetic field is specified by the exponent n and the separation angle θ_{max}, whereas the radiation from the disk is characterized by the cutoff radius r_{in}. By specifying these parameters we have fully determined the structure equations for the thin accretion disk, rotating in the black hole magnetosphere.

3.4.3 Special case: jet with no magnetosphere

Here we consider the radiatively truncated thin disk scheme introduced in the disk-jet-hole symbiotic model without magnetosphere. If no torque is exerted on a Keplerian disk by the rotating hole we have $c_L = 0$ and $c_E = 0$. Then the flux integral (54) simplifies to

$$F_{tot} = F = -\frac{\dot{M}_0}{4\pi r}\frac{\Omega_{,r}}{(\widetilde{E}-\Omega\widetilde{L})^2}\int_{\max(r_{ms},r_{in})}^{r}(\widetilde{E}-\Omega\widetilde{L})\widetilde{L}_{,r}dr\ , \quad (55)$$

where F is given by Eq. (A3) again, but with the substitution $x_{ms}^2 \to \max(r_{ms}, r_{in})/M$.

Falcke & Biermann (1995) have considered a direct connection between disk and jet, truncating the disk at values between $4M$ and $12M$. In our model the accretion disk does not power the jet directly, thus the inner edge of the accretion disk is at r_{ms}, but we suppress the radiation below r_{in}. Fig. 5 shows the radial distribution of the photon flux emitted from the surface of the disk with the radiative truncation at $r_{in} = 4M$, $8M$ and $12M$, for $a_* = 0$ (static case) and $a_* = 0.9982$ (at the spin limit of the canonical black hole). For rapid rotation the suppression of the radiation

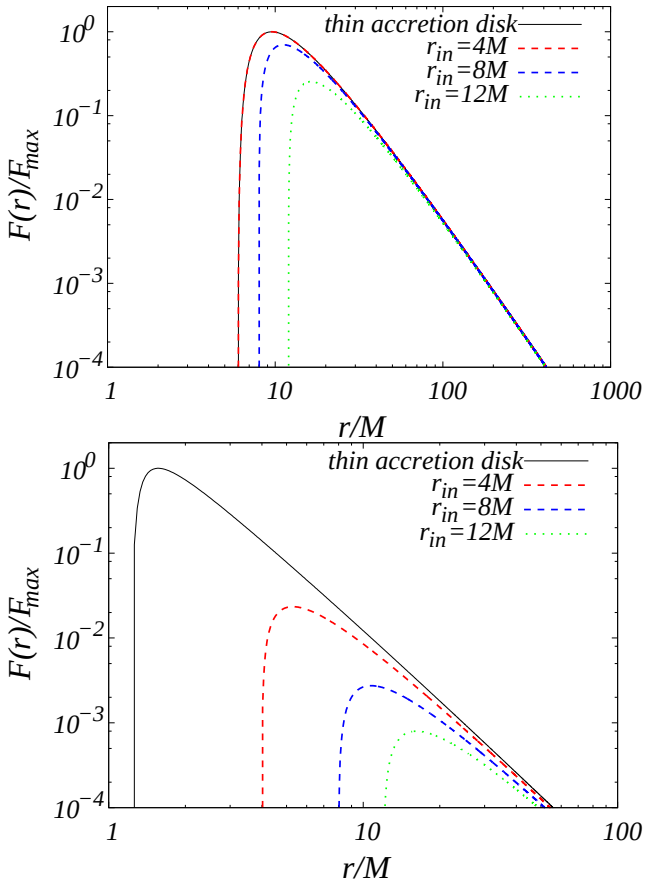

Figure 5. The time-averaged flux $F(r)$ radiated by a steady-state thin accretion disk about a Kerr black hole and by various truncated disk models with the nozzle radii $r_{in} = 4M$, $8M$ and $12M$. The upper plot is for zero spin, the lower plot for the maximally allowed spin $a_* = 0.9982$ of the canonical black hole. The flux is normalized to the maximal flux emitted from the thin accretion disk $F_{max} = 1.37 \times 10^{-5}\dot{M}_0/M^2$ for the static case and $F_{max} = 0.00498\dot{M}_0/M^2$ for the rotating black hole.

below r_{in} decreases the integrated flux considerably, provided $r_{in} > r_{ms}$. At low spin r_{ms} is larger than $4M$ and the radiative truncation only at $8M$ decreases the maximal value of $F(r)$. This behaviour is illustrated in Fig. 5.

3.4.4 Special case: magnetosphere with no jet

Considering solely the magnetic torque exerted on a Keplerian disk by the spinning black hole (no jet, $r_{in} = r_{ms}$), the expressions (47), (48) inserted in Eqs. (52), (53) give $c_L = \Omega c_E$. Then Eq. (54) leads to

$$F_{tot} = F + \frac{\dot{M}_0}{4\pi r}\frac{4}{\dot{M}_0}\frac{-\Omega_{,r}}{(\widetilde{E}-\Omega\widetilde{L})^2}\frac{M^2B_H^2}{\sqrt{\mathscr{A}(x_{ms})}} \times \int_{r_{ms}}^{\min(r,r_{max})}(\widetilde{E}-\Omega\widetilde{L})(\Omega^H-\Omega) \times \left(\frac{r}{r_{ms}}\right)^{1-n}\sqrt{\frac{\mathscr{A}}{\mathscr{D}}}\frac{r_+^2\sin^2\theta}{2M-r_-\sin^2\theta}dr\,. \quad (56)$$

The radial dependence of $\sin^2\theta$ is given by Eq. (49). In the expression (56) the photon flux depends on the magnetic field B_H and the parameter n used in in the power law (32).

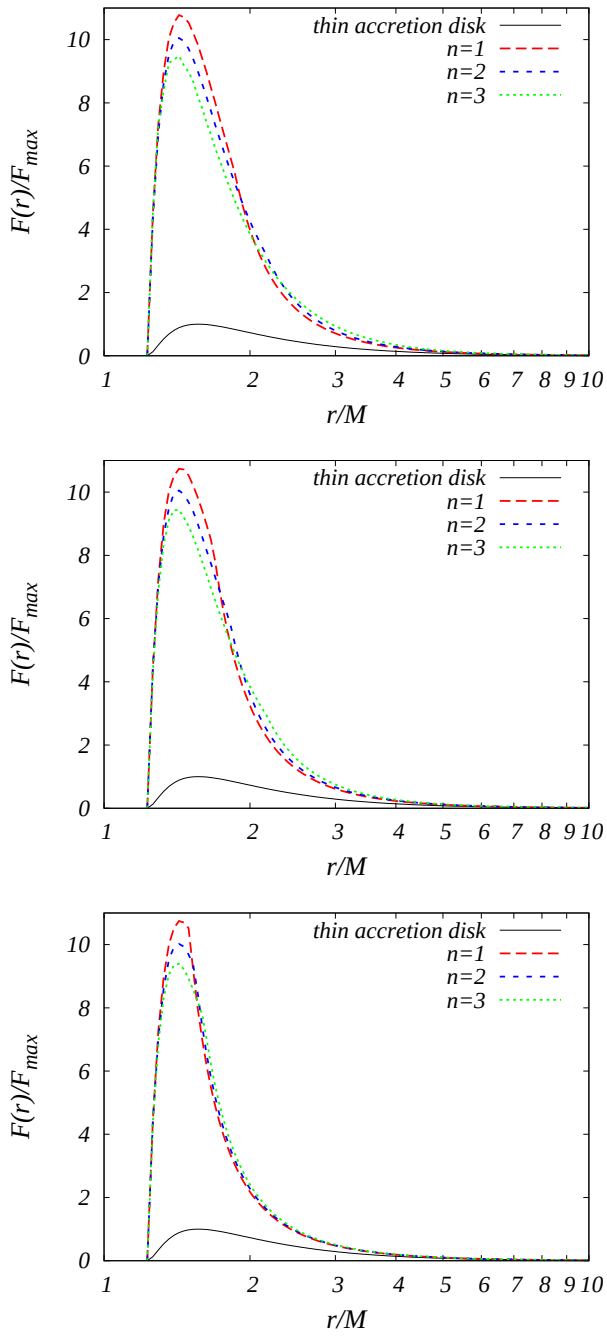

Figure 6. The time-averaged flux $F(r)$ radiated by an accretion disk around a rotating black hole ($a_* = 0.9982$) for the standard accretion disk and accretion disk with a magnetic torque. The angular boundary θ_{max} is set to $\pi/6$ (top), $\pi/4$ (middle) and $\pi/3$ (bottom). The parameter n takes the values 1,2 and 3. $F(r)$ is normalized with $F_{max} = 0.00498\dot{M}_0/M^2$.

In Fig. 6 we plotted the radial distribution of the photon flux determined by Eq. (56). In the plots the parameter n is set to 1, 2 and 3 whereas θ_{max} takes the values $\pi/6$, $\pi/4$ and $\pi/3$. This case differs from the discussion of Uzdensky (2005) by limiting the allowed range of θ_{max} to values > 0, so providing an additional free parameter in the boundary condition; this is the topology required by a jet. With in-

creasing values of θ_{max} we decrease the angular boundary of the closed magnetic field lines, which decreases the contribution of the torque conveyed by the flux lines to the emitted energy of the disk. For larger values of θ_{max} the flux profiles fall more steeply at higher radii. The increment of the parameter n decreases the radial fall-off of the magnetic field strength. Then the fall-off of the flux profile at higher radii is somewhat less steeper, as seen in the uppermost plot.

4 BLACK HOLE EVOLUTION AND ENERGY CONVERSION EFFICIENCY

4.1 Black hole mass and spin evolution equations

4.1.1 Canonical black hole

In Bardeen's accretion model the time derivatives of the total mass and angular momentum of the black hole are proportional to the specific energy $\widetilde{E}_{ms}$ and specific angular momentum $\widetilde{L}_{ms}$, respectively, of the particles falling in from the marginally stable orbit, the proportionality factor being in both cases the rate of change of the rest mass. Page & Thorne (1974) modified these relations by including the radiation emitted by the disk and captured by the black hole, to get:

$$dM/dt = \dot{M}_0\widetilde{E}_{ms} + (dM/dt)_{rad}\,, \quad (57)$$

$$dJ/dt = \dot{M}_0\widetilde{L}_{ms} + (dJ/dt)_{rad}\,. \quad (58)$$

From Eqs. (14) and (15) evaluated at r_{ms} one obtains $\widetilde{E}_{ms}$ and $\widetilde{L}_{ms}$. The time averaged rates $(dM/dt)_{rad}$ and $(dJ/dt)_{rad}$ at which photons carry energy and angular momentum into the black hole were computed by integrating the photon flux F over the disk surface in the Kerr potential (Thorne 1974), given here as Eqs. (A1) and (A2) of Appendix A. The evolution equations of the spin parameter a_* and of the total black hole mass M therefore can be rewritten as

$$\frac{da_*}{d\ln(M/M_1)} = \frac{1}{M}\frac{\widetilde{L}_{ms} + \dot{M}_0^{-1}(dJ/dt)_{rad}}{\widetilde{E}_{ms} + \dot{M}_0^{-1}(dM/dt)_{rad}} - 2a_*\,, \quad (59)$$

$$\frac{dM}{dM_0} = \widetilde{E}_{ms} + \dot{M}_0^{-1}(dM/dt)_{rad}\,, \quad (60)$$

where M_1 represents a mass scale, chosen as unity in what follows. Despite appearances, the right hand side of Eq. (59) does not depend on either the black hole mass M or the accretion rate $\dot{M}_0$. Indeed, from Eqs. (14) and (15) $\widetilde{L}_{ms} \propto M$, while $\widetilde{E}_{ms}$ does not depend on either M or $\dot{M}_0$. Since $F(r) \propto \dot{M}_0/M^2$, according to the integrals (A1) and (A2) $(dM/dt)_{rad} \propto \dot{M}_0$ and $(dJ/dt)_{rad} \propto \dot{M}_0 M$ hold, respectively. Then the right hand side of Eq. (59) depends solely on a_*, the differential equation becoming separable. Also, the extremum $da_*/d\ln M = 0$ does not depend on either M or $\dot{M}_0$.

Further, as Eq. (59) does not depend on the mass accretion rate, neither does the evolution $a_*(M)$. However, the evolution in time depends on $\dot{M}_0$, cf. Eqs. (57)-(58). As black holes of few solar masses and supermassive galactic black holes exhibit huge differences in $\dot{M}_0$, both their mass and spin evolutions occur at different characteristic time scales.

A similar analysis of Eq. (60) shows that dM/dM_0 does not depend on M or $\dot{M}_0$ either, but only on a_*.

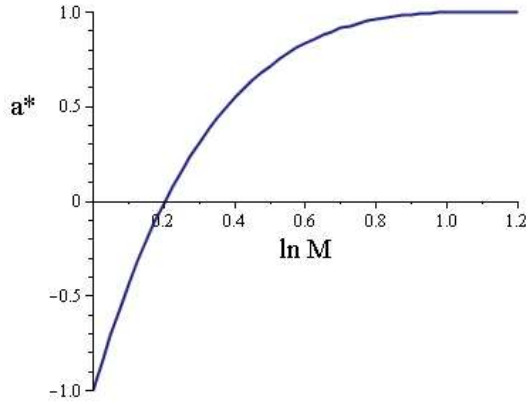

Figure 7. The variation of the spin parameter a_* due to standard accretion only in terms of the mass (taken in units of the initial mass). For convenience the counterrotation is represented by negative values of a_*. The graph is for initially counterrotating accreted particles. This slows down, then stops the rotation of the black hole, after which, in a corotating configuration the black hole spins up again in the opposite sense. The initial radius of the innermost stable circular geodesic orbit is $r_{ms} = 9M$ for counterrotating particles in the extreme Kerr geometry. When the rotation stops, $r_{ms} = 6M$ (Schwarzschild case). Finally when the black hole reaches maximal rotation in the opposite sense, $r_{ms} = M$. In the process the mass of the black hole is trebled (and it is 22% over the initial mass when it passes through the Schwarzschild state). Further accretion increases only the mass, not the dimensionless spin.

4.1.2 Black hole spin reversal due to accretion in Bardeen's model

We show explicitly here, how the spin evolves as function of mass in the simplest, Bardeen approximation (without corrections due to photon capture, magnetic fields and truncation of radiation). For this, we integrate Eq. (59), with the radiative contributions left apart. By employing the definitions (14) and (15) we get

$$\frac{\pm da_*}{d\ln M} = \frac{x_{ms} \mp 2a_* \pm 2a_* x_{ms}^{-2} - a_*^2 x_{ms}^{-3}}{1 - 2x_{ms}^{-2} \pm a_* x_{ms}^{-3}}\,, \quad (61)$$

with the upper (lower) sign referring to corotating (counterrotating) accreting particles on the innermost marginally stable circular geodesic orbit.

The numerical analysis of the system (61), (23) shows that counterrotating particles first reduce fast the rotation parameter to zero (the mass gain being 22%), after which the rotation is again increased by the corotating accretion up to the maximally rotating, extreme Kerr limit (the mass being trebled). This is shown on Fig. 7. This evolution is slightly changed by the various effects considered in the present paper.

4.1.3 Symbiotic model

In the generic case we take into account a) the torque $d\Delta L^D/dt$, b) the extracted power P^D due to the the magnetic coupling of the disk and the hole, c) the loss of angular momentum $d\Delta L^H/dt$, and d) the energy loss P^H due to the BZ mechanism. For the time averaged rates $(dJ/dt)_{rad}$ and

$(dM/dt)_{rad}$ we use the flux integral (54) and write the evolution equations in the form

$$dM/dt = \dot{M}_0\widetilde{E}_{ms} + (dM/dt)_{rad} - P^H - P^D \,, \quad (62)$$

$$dJ/dt = \dot{M}_0\widetilde{L}_{ms} + (dJ/dt)_{rad} + d\Delta L^H/dt + d\Delta L^D/dt \,. \quad (63)$$

Similar evolution equations were given by Park & Vishniac (1988) and Wang, Xiao & Lei (2002). However Park & Vishniac considered a black hole magnetosphere with only open field lines; while the photon capture was ignored by both Park & Vishniac and Wang, Xiao & Lei. We obtain the evolution equations

$$\frac{da_*}{d\ln M} = \frac{1}{M}\frac{\widetilde{L}_{ms}+N_J}{\widetilde{E}_{ms}+N_M} - 2a_* \,, \quad (64)$$

$$\frac{dM}{dM_0} = \widetilde{E}_{ms} + N_M \,, \quad (65)$$

with

$$N_J \equiv \dot{M}_0^{-1}[(dJ/dt)_{rad} + d\Delta L^H/dt + d\Delta L^D/dt] \,, \quad (66)$$

$$N_M \equiv \dot{M}_0^{-1}[(dM/dt)_{rad} - P^H - P^D] \,. \quad (67)$$

These equations contain the jet parameter r_{in}, and the parameters n, θ_{max} of the magnetosphere. The spin limit of the generalized equation (64) is independent of the mass scale and the accretion rate as in the case of the evolution equation (59) of a_*. This can be concluded from the relations $d\Delta L^H/dt \sim \dot{M}_0 M$, $d\Delta L^D/dt \sim \dot{M}_0 M$, $P^H \sim \dot{M}_0$ and $P^D \sim \dot{M}_0$ which give $N_J \sim M$ and render N_M independent of M and $\dot{M}_0$.

4.2 Radiative truncation of the disk

We present the evolution of the black hole mass and spin in the disk-jet-hole symbiotic models without magnetosphere in Fig. 8, for the sequence of nozzle radii $r_{in} = 4M$, $8M$ and $12M$, both for accretion disks with isotropic emission of radiation and electron scattering atmosphere.

For zero initial value of a_* the mass accretion with $0 \leqslant (M_0 - M_{0i})/M_{i0} \lesssim 1.3$ increases both the total mass and the spin of the black hole and the mass evolution is essentially independent of the photon capture. Here M_0 represents the rest mass of the black hole, which includes the accreted mass. For $(M_0 - M_{0i})/M_{i0} \gtrsim 1.3$ the black hole has already reached the spin limit and thus can gain no additional rotational energy by accretion. However, the accreting rest mass further increases the total mass M of the black hole. At the spin limit r_{ms} and $\widetilde{E}_{ms}$ reach minimal values, as seen in Fig. 1 and Eq. (14), therefore the slope of the upper part of the mass evolution curves decrease. The photon capture $(dM/dt)_{rad}$ is becoming less important with increasing the truncation radius of the radiation from the disk and the slope of the curve will further decrease.

If the initial value of the spin parameter is 1, its value will change only slightly until the limit is reached. The radius r_{ms} and specific energy $\tilde{E}_{ms}$ also decrease somewhat before reaching their limiting values and the photon capture becomes more important. Thus in the mass regime $(M_0 - M_{0i})/M_{i0} \gtrsim 1.3$ all evolution curves of the mass for $a_{*i} = 1$ have identical slopes with the corresponding (same r_{in}) curves of the initially non-rotating configurations.

Table 1. The upper limit of the spin parameter a_* and the efficiency ϵ for a symbiotic model with a radiative truncation radius r_{in}. The values refer to isotropic emission (I) and electron scattering atmosphere (ES).

r_{in} $[M]$	a_* (I)	ϵ (I)	a_* (ES)	ϵ (ES)
4	0.9999106	0.383	0.9999480	0.389
8	0.9999959	0.408	0.9999981	0.411
12	0.9999995	0.415	0.9999998	0.417

The spin evolution is also represented in Fig. 8. The surface of the disk and the corresponding energy flux decrease by increasing the radiative truncation radius. $(dM/dt)_{rad}$ becoming smaller, renders the evolution of the total black hole mass more close to Bardeen's law. For the highest radiative truncation radius considered, $r_{in} = 12M$ the spin limit is almost 1, similarly to the extreme Kerr holes without photon capture. This is an indication that only a negligible number of photons is captured by the hole, or otherwise stated, confirms the common-sense expectation, that the majority of the captured photons are emitted quite close to the gravitational radius. The limiting values of a_* are given in Table 1 for both the isotropic and electron scattering models.

The efficiency for converting accreted mass into outgoing radiation is

$$\epsilon = 1 - \dot{M}_0^{-1} dM/dt = 1 - \widetilde{E}_{ms} - \dot{M}_0^{-1}(dM/dt)_{rad} \,. \quad (68)$$

Canonical black holes for isotropic emission and electron scattering atmosphere have $\epsilon = 0.302$ and $\epsilon = 0.308$, respectively (Thorne 1974). In Table 1 we give the values of ϵ, considerably increased due to the jet. For $r_{in} = 4M$ the efficiency is close to 0.400, the value characterizing extreme Kerr black holes with photon capture. The explanation for this is that the specific energy $\widetilde{E}_{ms}$ in Eq. (68) is evaluated at a high spin limit. Increasing the radiative truncation radius ϵ exceeds 0.400, approaching 0.423, which is the efficiency of the extreme black Kerr hole without photon capture.

4.3 Magnetosphere models

In what follows we study the spin evolution for standard accretion disk models in the presence of a black hole magnetosphere. If the inner edge of disk is always at the marginally stable orbit then the only effects on the mass accretion are caused by the BZ mechanism and the torque conveyed from the hole to the disk via the magnetic field lines. These two effects have been studied separately by Park & Vishniac (1988) and Wang, Xiao & Lei (2002), respectively. We investigate numerically their combined effect and concentrate on the high spin regime.

In the evolution equations (64) and (65) the terms $d\Delta L^H/dt$, $d\Delta L^D/dt$, P^H and P^D of the torque and the extracted power are given by Eqs. (43), (44), (47) and (48) and the terms $(dJ/dt)_{rad}$ and $(dM/dt)_{rad}$ are determined by applying the flux integral (56). The efficiency for the conversion of the accreting mass into outgoing radiation defined

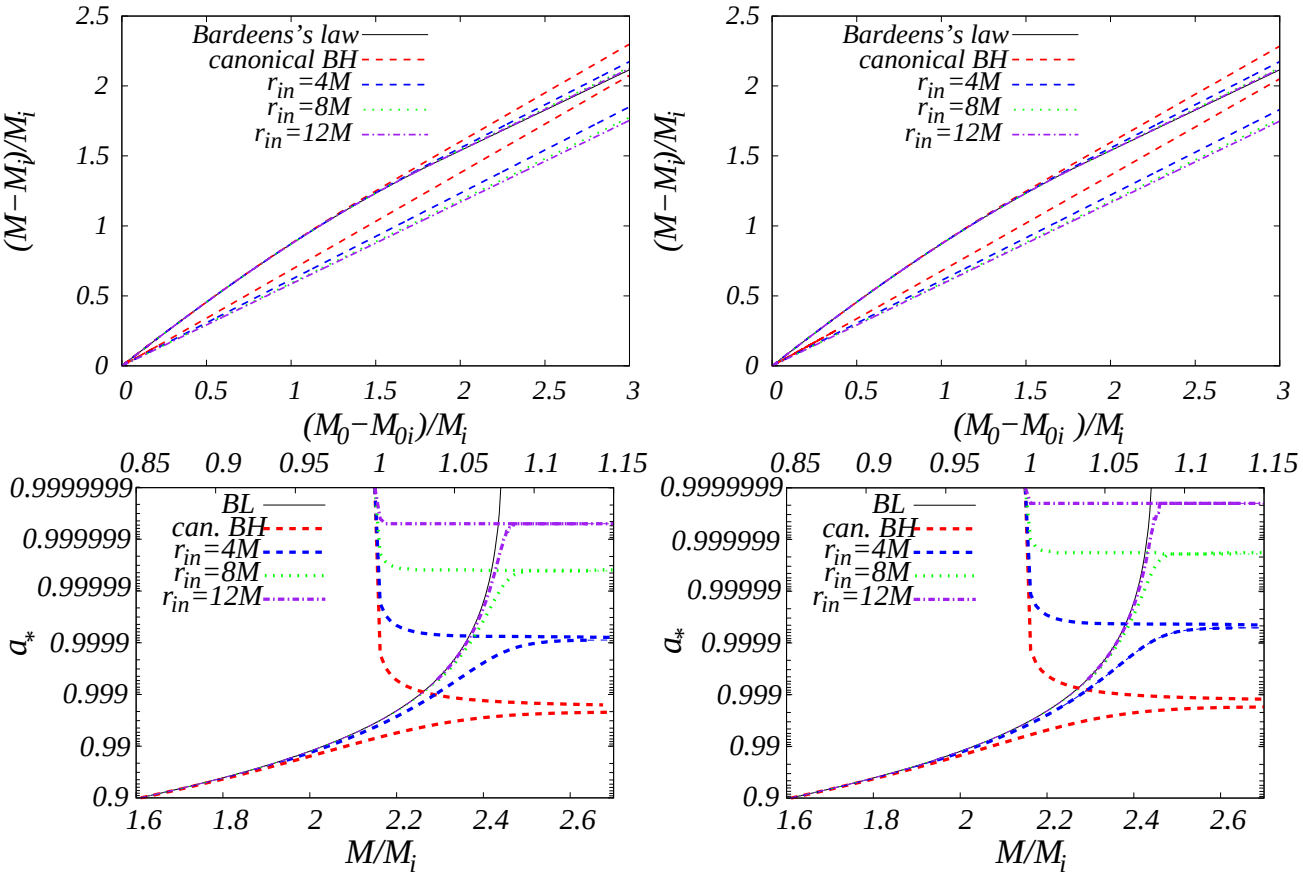

Figure 8. The effect of the jets (of radiative truncation) on the evolutions of the total mass-energy M (upper plots) and spin parameter a_* (lower plots) in the absence of the magnetosphere (generalization of Figs. 1 and 2 of Thorne 1974). M_i and M_{i0} are inital black hole total and rest masses. Left panel models are with isotropic disk emission; right panel models are with electron scattering atmosphere. Black curves represent Bardeen evolutions (no photon capture, initially non-rotating black holes). The two limiting cases of canonical black holes (allowing accretion and photon capture) are the dashed red curves (lower curve on mass evolution: initially extreme Kerr $a_{*i} = 1$; upper curve on mass evolution: initially non-rotating $a_{*i} = 0$). Similar evolutions are depicted for the radiative truncation radii $r_{in} = 4M$, $8M$ and $12M$. All evolutions with $a_{*i} = 0$ exhibit an initially faster increase of mass than in the Bardeen case, while mass increase for $a_{*i} = 1$ is slower. The rotation parameter on the vertical axis is represented on the $log_{10}(0.1/(1 - a_*))$ scale; there are two mass scales indicated on the horizontal axis, one for each of the initially non-rotating and extreme Kerr configurations. The jets (the truncation of radiation) renders the spin limit closer to the extreme Kerr case.

by Eq. (68) takes the form

$$\epsilon = 1 - \widetilde{E}_{ms} - N_M \ . \tag{69}$$

4.3.1 Open magnetic field lines from the horizon

If we consider the BZ mechanism and no closed magnetic field lines ($d\Delta L^D/dt = 0$ and $P^D = 0$), the only parameter left is the boundary angle θ_{max} of the open lines on the event horizon. By increasing θ_{max} we also increase the total area of the flux tube formed by the open field lines on the horizon. As a result, the torque exerted on the flux tube by the black hole raises and more rotational energy is extracted from the hole in the BZ process. This reduces the spin limit, which is presented in Table 2 and in Fig. 9. The extracted power P^H takes larger values when we increase the horizontal area of the open field lines even at smaller values of the spin limit. For lower values of spin parameter the mass-energy flux $(dM/dt)_{rad}$ becomes smaller as well and these effects decrease the term N_M in the mass evolution equation. Nevertheless, it is compensated by the higher values of $\widetilde{E}_{ms}$ taken at the lower spin limits. The net effect is that the slopes of the mass evolution curves are steeper with the increasing boundary angle θ_{max} and more total mass is produced by the same amount of the accreted rest mass, as seen in Fig. 9. The efficiency ϵ given in Table 2 also exhibits a behaviour similar to the one of the spin limit. With the increasing area of the flux tube formed by the open magnetic field lines the BZ process reduces the conversion efficiency of the accreted mass into radiation. Park & Vishniac (1988) applying a maximally efficient BZ mechanism and a constant accretion rate in their analysis demonstrated that a_* is decreasing in time and the black hole will spin down from the initial value $a_{*i} \approx 1$. Comparing their findings with our result, we can state that the extremely rapidly rotating black holes with $a_* \approx 1$ will slow down to the spin limits shown in Table 2 for the given boundary angles θ_{max}.

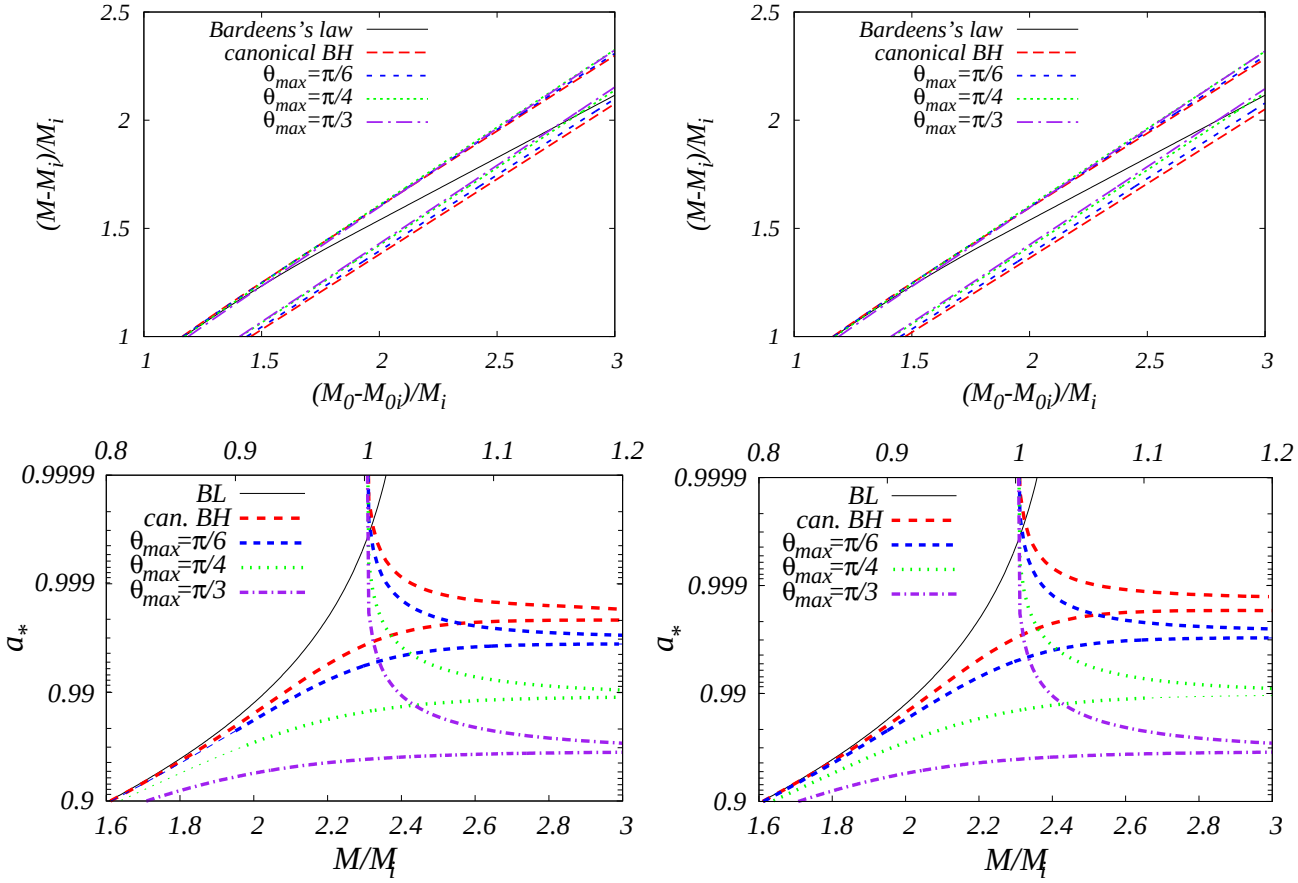

Figure 9. The evolution of the total mass-energy M (upper plots) and spin parameter a_* (lower plots) for a black hole with the inclusion of the BZ mechanism. Left hand panels show M and a_* for isotropic disk emission; right hand panels display the same plots for the electron scattering atmosphere.

Table 2. The limit of the spin parameter a_* and the efficiency ϵ of the accretion process in the presence of open magnetic field lines (BZ mechanism) for different boundary angles θ_{max}.

θ_{max}	a_* (I)	ϵ (I)	a_* (ES)	ϵ (ES)
$\pi/6$	0.9964	0.300	0.9969	0.307
$\pi/4$	0.9891	0.286	0.9897	0.290
$\pi/3$	0.9651	0.276	0.9657	0.281

4.3.2 Closed magnetic field lines

By switching the BZ process off ($d\Delta L^H/dt = 0$ and $P^H = 0$), we can study the effects of the magnetic torque exerted on the accretion disk by the black hole. The area of flux tube formed on the horizon by the closed field lines connecting the disk to the hole is determined by the angle θ_{max} again but it is now decreasing with the increasing boundary angle. The effect of the magnetic coupling between the hole and the disk becomes smaller for greater values of θ_{max}, as opposed to the BZ process. This can be seen in Table 3 containing the spin limits and the efficiency for different values of θ_{max} and n. As we increase θ_{max} for a fixed n we obtain higher spin limits approaching the limiting values of the canonical black holes. The highest values derived for $\theta_{max} = \pi/3$ are still somewhat smaller than 0.9978 (isotropic emission) and 0.9982 (electron scattering atmosphere). The efficiency also follows the same tendency: for $\theta_{max} = \pi/6$ the efficiency ϵ is smaller than 0.302 (isotropic emission) and 0.308 (electron scattering atmosphere) obtained for the standard accretion disks but approaches and somewhat exceeds those values with increasing θ_{max}. Although for a fixed θ_{max} the maximal flux emitted by the disk and the number of the captured photons are reduced if we increase the exponent n, the quantities $d\Delta L^D/dt$ and P^D compensate the diminishing effects of $(dJ/dt)_{rad}$ and $(dM/dt)_{rad}$. As a result, the spin limits decrease for higher values of n, deviating more from those of the canonical black hole. Fig. 10 presenting the mass and spin evolution of the black hole demonstrates this kind of dependence of the limiting values on the parameters of the magnetic fields. For $\theta_{max} = \pi/6$ and $n = 3$ the mass evolution is faster than in the case of the canonical black hole because of the relatively high value of $\widetilde{E}_{ms}$ at the lower spin limit but the magnetic coupling of the hole and the disk becomes more dominant with decreasing boundary angle and reduces the mass evolution rate of the hole. Any decrease in the exponent n also causes a reduction in the mass evolution rate. Wang, Xio & Lei (2002, 2003) already analyzed the black hole evolution in the magnetically coupled model for the parameters $0 < \theta_{max} < \pi/2$ and $1 < n < 6$. They obtained the same trends of the spin limit by varying n for

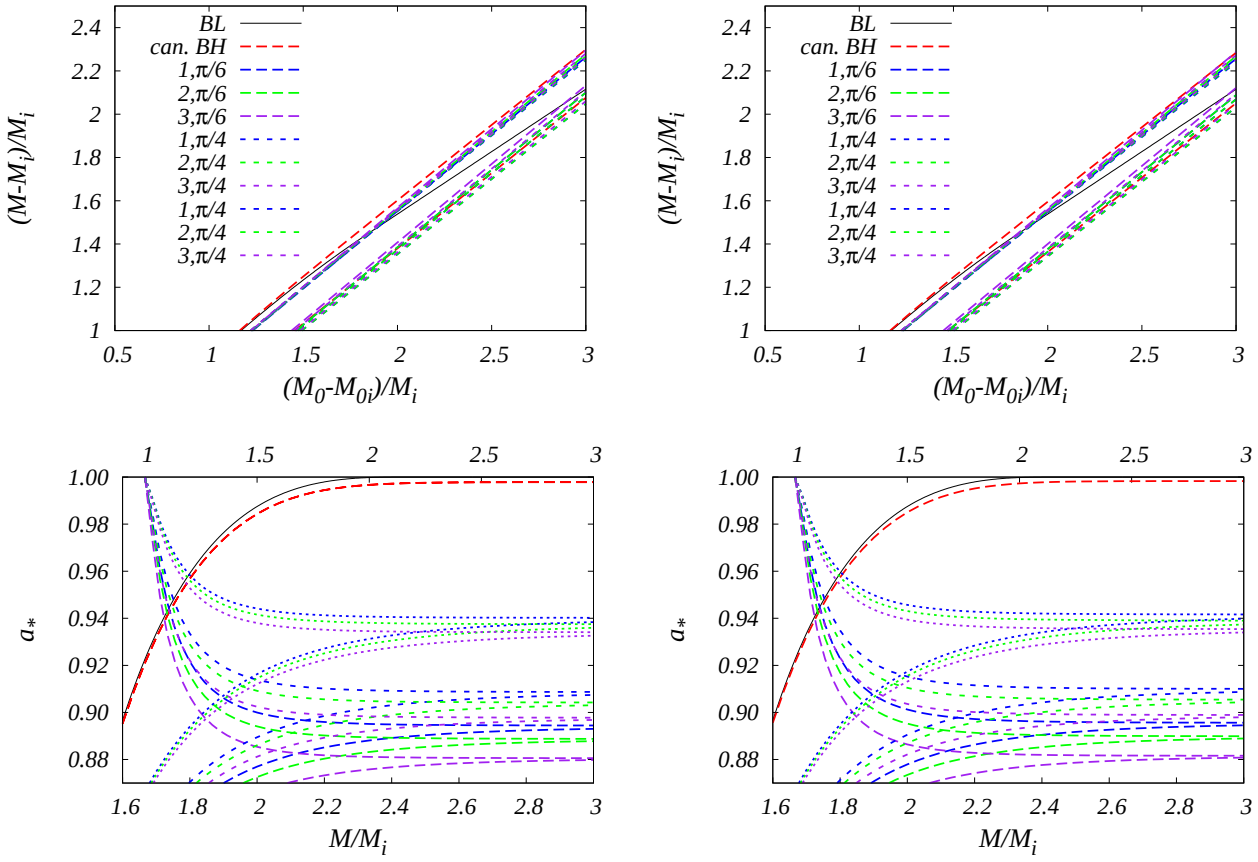

Figure 10. The evolution of the the total mass-energy M (upper plots) and the spin parameter a_* (lower plots) for a black hole, with the inclusion of the magnetic torque exerted on the disk by the hole. The integer numbers refer to n, the angles to $\theta_{\max}$. Left hand panels show M and a_* for isotropic disk emission, right hand ones display the same plots for electron scattering atmosphere. Linestyles in the lower plots are as for the upper plots.

Table 3. The spin limits a_* and the efficiency ϵ for the accretion process in black hole magnetosphere with closed field lines for different boundary angles θ_{max} and magnetic field strength power law exponents n.

θ_{max}	n	a_* (I)	ϵ (I)	a_* (ES)	ϵ (ES)
$\pi/6$	1	0.8944	0.291	0.8956	0.294
	2	0.8887	0.284	0.8899	0.288
	3	0.8807	0.275	0.8817	0.278
$\pi/4$	1	0.9086	0.296	0.9100	0.300
	2	0.9042	0.291	0.9053	0.295
	3	0.8980	0.284	0.8991	0.287
$\pi/3$	1	0.9400	0.308	0.9416	0.313
	2	0.9374	0.305	0.9389	0.309
	3	0.9342	0.301	0.9356	0.305

fixed values of θ_{max}, even if they neglected the photon capture effect decreasing the limiting value of a_*.

4.3.3 Combined open and closed magnetic field line topology

A complete black hole magnetosphere model contains both the open and the close flux lines emanating from the event horizon. Hence both the BZ mechanism and the torque produced by the hole on flux lines anchored in the accretion disk affect on the evolution characteristics of the rotating black hole. In the second part of Table 4 we present the spin limits and the efficiency for the combined effect of the BZ mechanism and the magnetic torque. Here we see that the limiting values of a_* deviate more from the values obtained for canonical black holes than without the BZ mechanism included. Since the variation of θ_{max} increases the area of the flux tube with open (closed) field line topology and the same time decreases the area of the flux tube with the closed (open) one, the separation angle θ_{max} determines if the BZ process or the magnetic coupling of the black hole to the disk has a more dominant role. Therefore, the BZ mechanism produces only a weak effect for $\theta_{max} = \pi/6$ and a relatively small decrease in the spin limit compared with the values for the magnetic coupling. For $\theta_{max} = \pi/3$ the contribution of the BZ mechanism is stronger and so is the reduction in the limiting values of the spin. An increasing parameter n reduces the spin limit and the efficiency, an

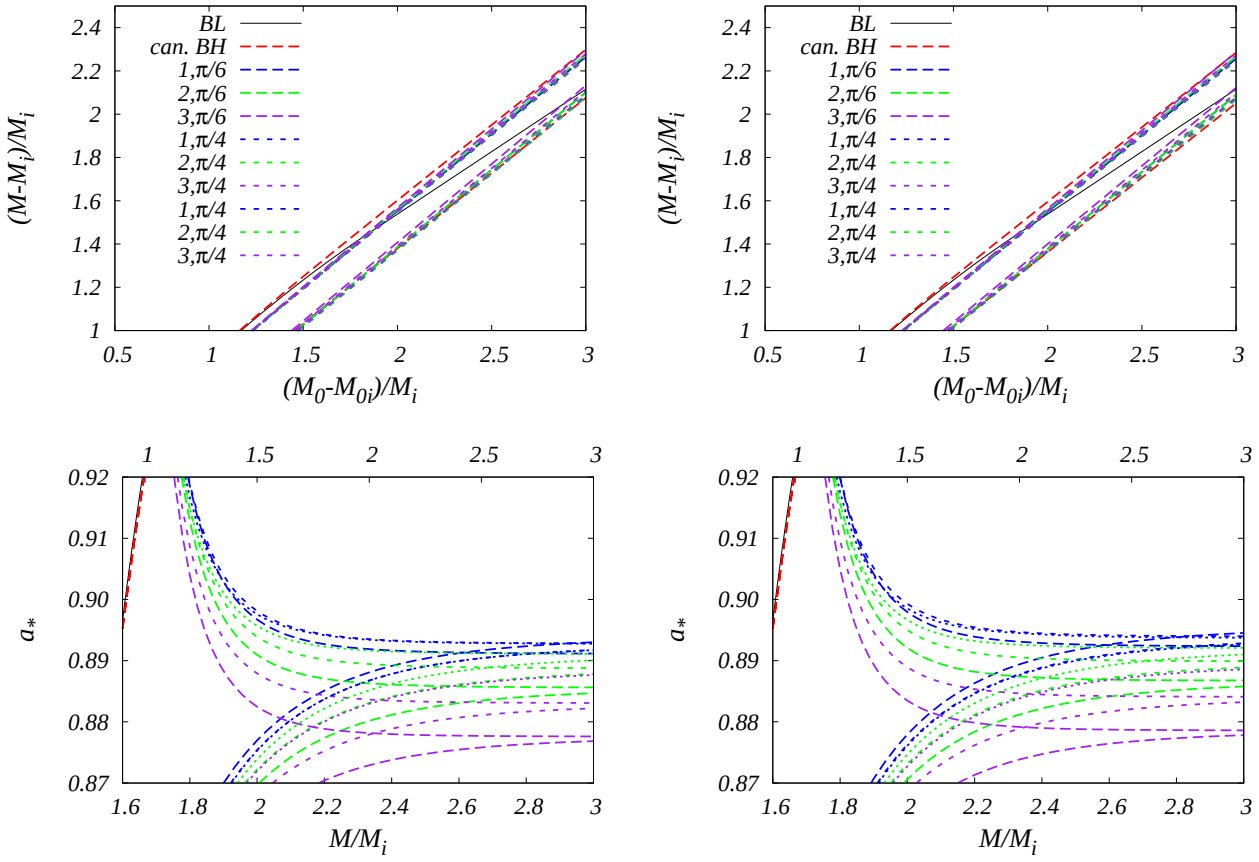

Figure 11. The evolution of the the total mass-energy M (the upper plots) and the spin parameter a_* (the lower plots) for a black hole with the inclusion of the BZ mechanism and the magnetic torque exerted on the disk by the hole. Left panel has M and a_* for an isotropic disk emission; right panel for the electron scattering atmosphere. Linestyles in the lower plots are as for the upper plots.

Table 4. The spin limit a_* and the efficiency ϵ for the accretion process in black hole magnetosphere with combined open and closed magnetic field topology, for various boundary angles θ_{max} and magnetic field strength power law exponents n.

θ_{max}	n	a_* (I)	ϵ (I)	a_* (ES)	ϵ (ES)
$\pi/6$	1	0.8911	0.290	0.8923	0.294
	2	0.8856	0.284	0.8867	0.287
	3	0.8777	0.274	0.8787	0.278
$\pi/4$	1	0.8928	0.293	0.8939	0.296
	2	0.8887	0.288	0.8899	0.292
	3	0.8832	0.282	0.8842	0.285
$\pi/3$	1	0.8927	0.296	0.8937	0.298
	2	0.8911	0.293	0.8920	0.296
	3	0.8887	0.291	0.8897	0.293

effect which increases with the value of θ_{max} (largest for $\theta_{max} = \pi/6$). Fig. 11 shows the evolution of the black hole parameters. The trends in the mass evolution are the same as for the magnetic coupling case but the differences in the steepness of the mass evolution curves are moderated by the BZ mechanism.

4.4 Symbiotic model with magnetosphere

In this subsection we combine the effect of the open and closed magnetic field topology with the radiative truncation of the disk emerging from the symbiotic model.

The truncation of the radiation from the disk (determined by r_{in}) reduces the effect of the photon capture by the black hole and brings the accretion process closer to Bardeen's evolution law. However, the BZ mechanism and the extraction of mass-energy and rotational energy of the hole via the closed field lines are more important effects. In particular, the magnetic torque of the closed magnetic field lines typically reduce the spin limit to values at about 0.89, as is seen on Fig. 12. Table 5 shows the new numbers, and the difference with respect to the numbers of Table 4 is but a slight increase due to the radiative truncation.

For a powerful jet such a low value of the spin is forbidden by arguments on the pion decay. As the severe decrease in the final spin is due to the torque of the closed magnetic field lines coupling to the very inner region of the disk, one could speculate why the contribution of the closed magnetic field lines is disfavoured by observations. One possibility is that the inner region of the disk (hence the associated closed magnetic field torque) is missing. This could arise for example if the central Kerr black hole is replaced by a binary black hole merger (Liu and Shapiro 2010), such that tidal

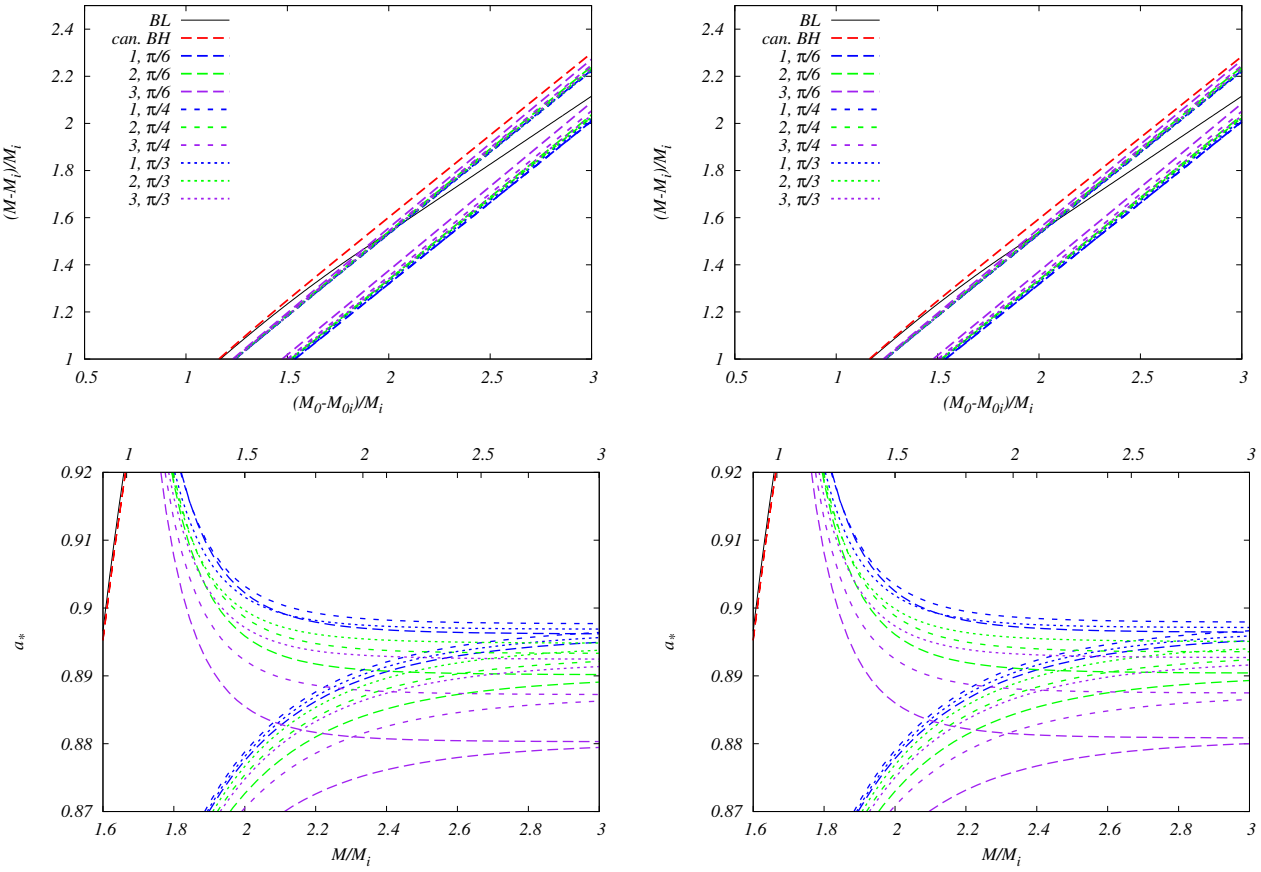

Figure 12. The evolution of the the total mass-energy M (upper plots) and the spin parameter a_* (lower plots) for the symbiotic model with black hole magnetosphere and $r_{in} = 4M$. For the curves running above the black curve indicating Bardeens's law (BL) the initial value of a_* is zero. With the initial value of 1 we obtained the curves running below the black curve. Left panel has M and a_* for an isotropic disk emission; right panel for the electron scattering atmosphere.

torques acting on the gaseous accretion disk around the binary create a gap in the disk. The closed magnetic field lines could also decouple from the disk, slipping along the accreting plasma and exerting a much smaller torque on the disk, as discussed in McKinney and Narayan (2007). Or alternatively the inner disk can decouple from the outer disk, being spun up by the black hole and then swallowed whole, following which a new inner disk is built up (similarly to the Biermann & Hall (1973) model, where a temporary storage of angular momentum in a disk ring was employed). The most radical option would be to forbid the closed magnetic field lines connecting the horizon to the disk, all magnetic field lines (emanating from both the horizon and the disk) being open.

We present the mass accretion and the spin limit for the symbiotic model with only open magnetic field line contribution on Fig. 13 and Table 6. The numbers are close to those given in Table 2 (referring to the open magnetic field lines, with the whole disk radiating), but slightly increased by the radiative truncation, as expected.

Since the effect of the closed field lines is sensitive to the parameter n only in the very inner region (which was decoupled), the results are independent of the model parameter n. Then only the variation of the angular boundary θ_{max} of the open field lines, affects the limiting values of a_*. These spin limits are given in Table 6. For $r_{in} = 8M$ and $12M$ they tend to be identical, indicating that the photon capture from the regions closer to the horizon is more important. With increasing θ_{max} we strengthen the effects due to the BZ process and decrease the spin limits, also indicated by the numbers of Table 2.

For wider solid angle of the open field lines the mass evolution are steeper. Nonetheless, the mass evolution curves with increasing θ_{max} are approaching the evolution profile of the canonical black hole because the increase of the radiative truncation radius compensates the effect of the BZ mechanism. For higher radii r_{in} the mass evolution curves are also steeper.

The efficiency ϵ shown in Table 6 is slightly decreasing for higher values of θ_{max} as more and more rotational energy is extracted by the BZ process. The trends characterizing the pure symbiotic model are also present where the increasing radiative truncation radius causes in the value of ϵ a mild increase. Thus in symbiotic models combined with black hole magnetosphere we can produce conversion efficiencies higher than those obtained for the canonical black holes if the angle θ_{max} is small enough. For greater boundary angles, such as $\theta_{max} = \pi/3$, the canonical black holes are still more efficient in the mass-to-radiation conversion mechanism. The truncation effect here is not so important,

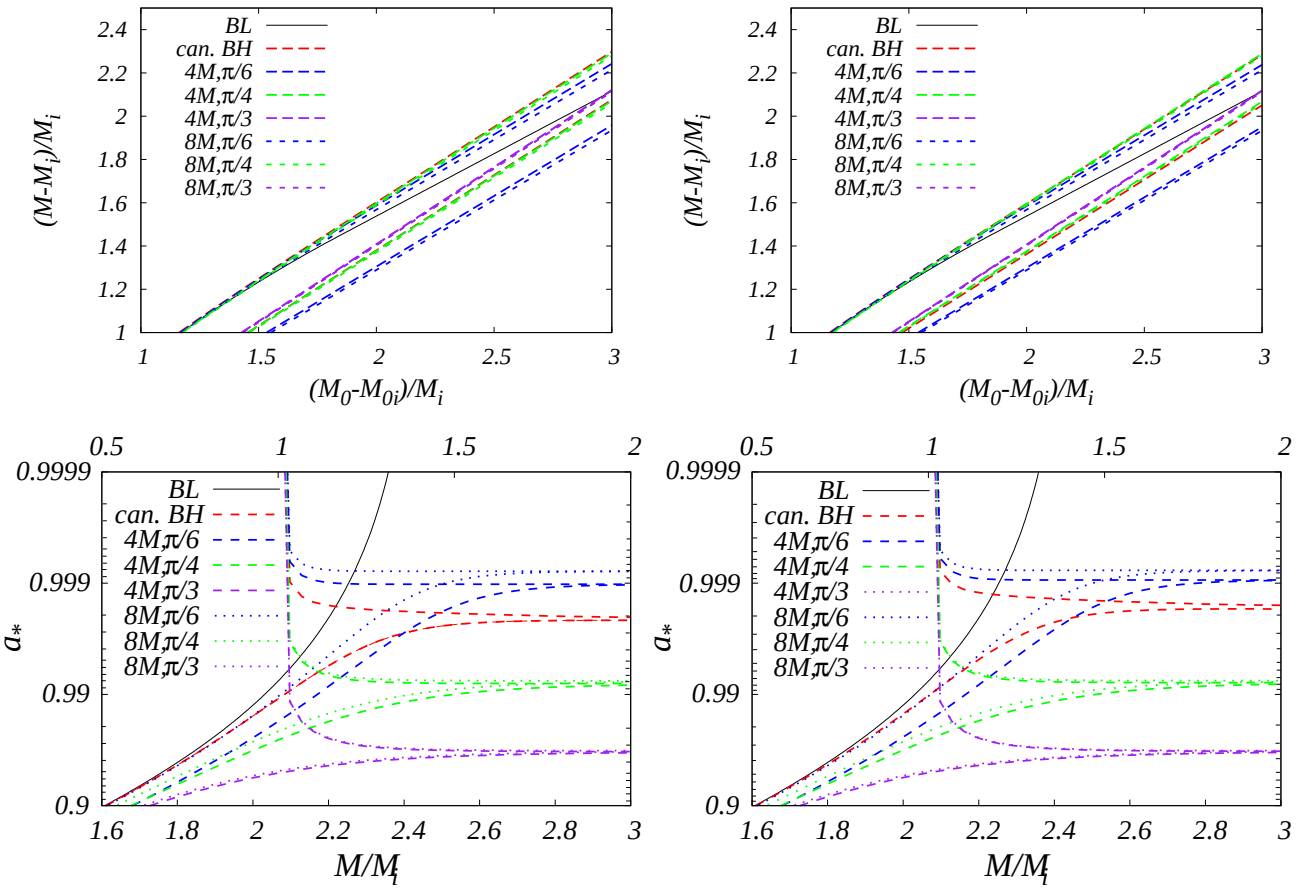

Figure 13. The evolution of the the total mass-energy M (upper plots) and the spin parameter a_* (lower plots) for the symbiotic model with open magnetosphere topology and radiative truncation radius $r_{in} = 4M$ and $8M$. For the curves running above the black curve representing Bardeens's law (BL) the initial value of a_* is zero. With the initial value of 1 we obtain the curves running below the black curve. Left panel has M and a_* for an isotropic disk emission; right panel for the electron scattering atmosphere.

though ϵ can be increased somewhat by applying greater values for r_{in}.

5 CONCLUSION

In this paper we explored a black hole - accretion disk - magnetosphere - jet symbiotic model, consistent with the observations on the accretion disk and on jet. The thin, steady-state accretion disk feeds the black hole in both angular momentum and mass. Observations of the source GRS1915+105 indicate that the innermost region of the disk does not radiate when the jet is powerful. (The initial Lorentz factors of jet flows can be very large, of order $\gtrsim 50$.) Hence we assume no radiation below a certain radius, as opposed to the exterior luminous part of the disk. The surplus of energy and angular momentum transported via accretion into the black hole can be regarded as a source of the strong jet.

The jet is driven purely electromagnetically by the black hole rotation. We assumed that the jet starts as a Poynting flux, carrying no baryonic matter, which is added into the jet only far up from the black hole by intersecting clouds, stars, stellar winds and from shear and boundary instabilities. Thus, there is no direct connection between the disk and jet in this model, in agreement with observations on the long lifetime of jets. Due to the extremely long lifetime of a relativistic jet and its related inefficient spin-down, we could neglect the backreaction of the jet onto the black hole.

The magnetosphere consists of an open magnetic field region with field lines emanating from the polar regions of the black hole, exhibiting the Blandford-Znajek mechanism, responsible for powering the jets in AGN's and GRB's; a closed magnetic field region with field lines emanating from the horizon under a polar angle $\theta > \theta_{max}$ and anchored to the disk, thus exerting a torque on it; and finally an exterior open magnetic field line configuration, extending from $r > r_{\rm max}$ (the radius where the closed field lines emanating at θ_{max} are anchored), with no direct coupling to the black hole.

Under these assumptions we have studied the spin evolution of the black hole in its symbiosis with the accretion disk, jet and the black hole magnetosphere. The topology of the magnetic field has by far the most prominent role: it drastically modifies the number of the captured photons and in turn the spin evolution of the black hole. While for open field line topology the limiting values of the spin parameter and the conversion efficiency are slightly decreased as compared to the values derived for canonical black holes, the

Table 5. The spin limit a_* and the efficiency ϵ of the accretion process in symbiotic system with black hole magnetosphere for different boundary angles θ_{max} and magnetic field strength power law exponents n. The first set of nine lines shows a_* and ϵ when the radius r_{in} is set to $4M$; the second set of nine lines displays these quantities when $r_{in} \in (8M, 12M)$.

θ_{max}	n	a_* (I)	ϵ (I)	a_* (ES)	ϵ (ES)
$\pi/6$	1	0.8961	0.309	0.8964	0.309
	2	0.8901	0.301	0.8904	0.302
	3	0.8803	0.285	0.8808	0.267
$\pi/4$	1	0.8976	0.312	0.8979	0.312
	2	0.8933	0.306	0.8935	0.306
	3	0.8872	0.298	0.8874	0.298
$\pi/3$	1	0.8969	0.310	0.8971	0.311
	2	0.8948	0.308	0.8950	0.309
	3	0.8924	0.305	0.8927	0.306
$\pi/6$	1	0.8968	0.311	0.8969	0.311
	2	0.8901	0.302	0.8909	0.303
	3	0.8822	0.291	0.8825	0.292
$\pi/4$	1	0.8983	0.313	0.8984	0.314
	2	0.8939	0.308	0.8939	0.308
	3	0.8879	0.300	0.8879	0.300
$\pi/3$	1	0.8975	0.312	0.8976	0.312
	2	0.8955	0.311	0.8955	0.311
	3	0.8931	0.307	0.8931	0.307

Table 6. The upper limit of the spin parameter and the efficiency ϵ for the accretion process in a symbiotic system with black hole magnetosphere, but no coupling of the closed magnetic field lines to the disk below r_{in}. The notations are as for Table 2. The value of r_{in}, also representing the truncation radius of the radiation from the accretion disk is set to $4M$, $8M$ and $12M$. The parameter θ_{max} runs over the values $\pi/6$, $\pi/4$ and $\pi/3$.

$r_{in}[M]$	θ_{max}	a_* (I)	ϵ (I)	a_* (ES)	ϵ (ES)
4	$\pi/6$	0.9990	0.347	0.9991	0.350
	$\pi/4$	0.9920	0.307	0.9922	0.309
	$\pi/3$	0.9673	0.287	0.9675	0.288
8	$\pi/6$	0.9992	0.354	0.9992	0.353
	$\pi/4$	0.9925	0.311	0.9925	0.311
	$\pi/3$	0.9679	0.290	0.9679	0.290
12	$\pi/6$	0.9992	0.354	0.9992	0.354
	$\pi/4$	0.9925	0.311	0.9925	0.311
	$\pi/3$	0.9680	0.290	0.9680	0.290

inclusion of the closed magnetic field configuration lowers the spin limit considerably, from ˜0.998 to ˜0.89. This happens in spite of the size of the closed magnetic field shrinking with increasing spin. Thus the topological properties of the magnetic field strongly correlate with the spin limit.

Therefore, assuming that observations suggest that spins larger than 0.95 are common we confirm Hirose et al. (2004) and McKinney (2005) that the magnetic field configuration strongly connecting black hole and disk should be uncommon.

Therefore observations on black hole spins could favour or disfavour the existence (or the coupling to the disk) of the closed magnetic field line region. In particular, a high black hole spin, as would be inferred from the low energy cutoff of the electron energy distribution in the low radio frequency spectrum of the jet indirectly forbids the existence of such a closed magnetic field.

As for the jet contribution, we find that narrow opening angles led to larger spin limits, than for canonical black holes. The radiative truncation of the disk suggested by the presence of the jet further increases the spin limit. We conclude that collimated jets slightly increase both the spins and the efficiency.

ACKNOWLEDGMENTS

The authors would like to thank Alina-Cătălina Donea, Zoltán Keresztes and Li-Xin Li for discussions, and for Gábor Paragi and Tiberiu Harko for assistance in running the numerical codes in the early phases of this work. The collaboration between the University of Szeged and the University of Bonn was via an EU Sokrates/Erasmus contract and between the University of Szeged and Hong Kong University via the GRF grant No. 701808P of the government of the Hong Kong SAR. LÁG was supported by COST Action MP0905 "Black Holes in a Violent Universe", the Hungarian Scientific Research Fund (OTKA) grants nos. 69036 and 81364. Support for PLB was coming from the AUGER membership and theory grant 05 CU 5PD 1/2 via DESY/BMBF and VIHKOS.

APPENDIX A: BASIC FORMULAE OF THE PHOTON CAPTURE

The time averaged rates $(dM/dt)_{rad}$ and $(dJ/dt)_{rad}$ at which the photons leaving the disk carry energy and angular momentum to the event horizon are given by the integrals (Page & Thorne 1974)

$$\left(\frac{dM}{dt}\right)_{rad} = -4\pi \int_{r_{ms}}^{\infty}\int_0^{\pi/2}\int_0^{2\pi} n_t(r,\Theta,\Phi)C(\Theta,\Phi) \times S(\Theta)\cos\Theta\sin\Theta r F(r) d\Phi d\Theta dr \,, \quad \text{(A1)}$$

$$\left(\frac{dJ}{dt}\right)_{rad} = 4\pi \int_{r_{ms}}^{\infty}\int_0^{\pi/2}\int_0^{2\pi} n_\phi(r,\Theta,\Phi)C(\Theta,\Phi) \times S(\Theta)\cos\Theta\sin\Theta r F(r) d\Phi d\Theta dr \,. \quad \text{(A2)}$$

In the above integrands n_t and n_ϕ are components of the renormalized photon momentum:

$$-n_t = \mathscr{C}^{-1/2}(\mathscr{G} + x^{-1}\mathscr{D}^{1/2}\sin\Theta\sin\Phi) \,,$$
$$n_\phi = M\mathscr{C}^{-1/2}(x\mathscr{F} + x\mathscr{B}\mathscr{D}^{1/2}\sin\Theta\sin\Phi) \,,$$

C is the photon capture function of the photons radiated in the direction (Θ, Φ), taking the value 1 if the photons are captured by the hole and 0 if they escape to infinity. $S = 1/\pi$ stands for isotropic emission and $S = (3/7\pi)(1 + 2\cos\Theta)$ for electron scattering atmosphere. The photon flux

was expressed analytically (Page & Thorne 1974) as

$$
\begin{aligned}
F(x) \quad = \quad & -\dot{M}_0/(4\pi r(x))\frac{3}{2M}\frac{1}{x^2(x^3-3x+2a_*)} \\
& \times\left[x-x_{ms}+\frac{3}{2}a_*\ln\left(\frac{x}{x_{ms}}\right)\right. \\
& -\frac{3(x_1-a_*)^2}{x_1(x_1-x_2)(x_1-x_3)}\ln\left(\frac{x-x_1}{x_{ms}-x_1}\right) \\
& -\frac{3(x_2-a_*)^2}{x_2(x_2-x_1)(x_2-x_3)}\ln\left(\frac{x-x_2}{x_{ms}-x_2}\right) \\
& \left.-\frac{3(x_3-a_*)^2}{x_3(x_3-x_1)(x_3-x_2)}\ln\left(\frac{x-x_3}{x_{ms}-x_3}\right)\right] \ . \quad \text{(A3)}
\end{aligned}
$$

where $x_{ms}=\sqrt{r_{ms}/M}$, given by Eq. (23) and x_1, x_2 and x_3 are the roots of the equation $x^3-3x+2a_*=0$.

REFERENCES

Abramowicz M., Jaroszynski M. & Sikora M., *Astron. Astrophys.*, **63**, 221 (1978)
Agol E. & Krolik J. H., *Astrophys. J.* **528**, 161 (2000)
Afshordi N. & Paczyński B. *Astrophys. J.* **592**, 354 (2003)
Araudo A. T., Bosch-Ramon V., Romero G. E., *Astron. & Astrophys.* **522**, A97 (2010)
Armitage Ph. J. & Natarajan P., *Astrophys. J.*, **523**, L7 (1999)
Bardeen J. M., *Nature* **226**, 64 (1970)
Bardeen J. M., Press W. H., & Teukolsky S. A., *Astrophys. J.* **178**, 347 (1972)
Berti E. & Volonteri M., *Astrophys. J.* **684**, 822 (2008)
Biermann P. L. & Hall D., *Astron. & Astrophys.* **27**, 249 (1973)
Blandford R. D., *Month. Not. Roy. Astr. Soc.* **176**, 465 (1976)
Blandford R. D. & Znajek R. L., *Month. Not. Roy. Astr. Soc.* **179**, 433 (1977)
Blandford R. D. & Königl A., *Astrophys. J.* **232**, 34 (1979)
Blandford R. D. & Payne D. G. *Month. Not. Roy. Astr. Soc.* **199**, 883 (1982)
Camenzind M., *Astron. & Astrophys.* **156**, 137, *Astron. & Astrophys.* **162**, 32 (1986)
Camenzind M., *Astron. & Astrophys.* **184**, 341 (1987)
Chini R., Kreysa E., Biermann P. L., *Astron. & Astrophys.* **219**, 87 (1989)
Done C., Madejski G. M., & Życki P. T., *Astrophys. J.* **536**, 213 (2000)
Donea A. C. & Biermann P. L., *Astron. & Astrophys.* **316**, 43 (1996)
Duţan I., arXiv:1001.5434 (2010)
Eikenberry S. S., *Astrophys. J. Lett.* **494**, L61 (1998)
Faber S. M., Tremaine S., Ajhar E. A., et al. *Astron. J.* **114**, 1771 (1997)
Falcke H, in "Jets from Stars and Galactic Nuclei", Ed. W. Kundt, *Springer Lecture Notes* **471**, 19 (1996); astro-ph/9512093
Falcke H. & Biermann P. L., *Astron. & Astrophys.* **293**, 665 (1995)
Falcke H., Malkan M. A. & Biermann P. L., *Astron. & Astrophys.* **298**, 375 (1995)
Falcke H. & Biermann P. L., *Astron. & Astrophys.* **308**, 321 (1996)
Falcke H. & Biermann P. L., *Astron. & Astrophys.* **342**, 49 (1999)
Falcke H., Nagar N. M., Wilson A. S. & Ulvestad J. S., *Astrophys. J.* **542**, 197 (2000)
Fender R. P., *Month. Not. Roy. Astr. Soc.* **343**, .L99 (2003)
Gammie C. F., *Astrophys. J.* **522**, L57 (1999)
Ghisellini G., Tavecchio F., *Month. Not. Roy. Astr. Soc.* **386**, L28 (2008)
Gopal-Krishna, Biermann P. L., & Wiita P. J., *Astrophys. J. Lett.* **603**, L9 (2004)
Hirose, S., et al., textitAstrophys. J. **606**, 1083 (2004)
Hirotani K., Takahashi M., Nitta S., & Tomimatsu A., *Astrophys. J.* **386**, 455 (1992)
Hughes S. A. & Blandford, R. D. , *Astrophys. J.* **585**, L101 (2003)
Janiuk, A., Czerny, B., *Month. Not. Roy. Astr. Soc.* in press, E-print: arXiv:1102.3257 (2011)
Kormendy J. & Richstone D., *Annual Rev. of Astron. & Astrophys.* **33**, 581 (1995)
Krolik J. H., *Astrophys. J.* **515**, L73 (1999)
Li L. X., *Astrophys. J.*, **533**, L115 (2000)
Li L. X., *Phys. Rev.* **D 68**, 024022 (2003)
Liang E. T. P. & Price R. H., *Astrophys. J.* **218**, 247 (1977)
Liu Y. T. & Shapiro S. L., *Accretion Disks Around Binary Black Holes: A Quasistationary Model*, E-print: arXiv:1011.0002 (2010)
Macdonald D. A. & Thorne K. S., *Month. Not. Roy. Astr. Soc.* **198**, 345 (1982)
McKinney, J.C., *Astrophys. J. Lett.* **630**, L5 (2005)
McKinney, J.C., Narayan, R., *Month. Not. Roy. Astr. Soc.* **375**, 513, 531 (2007)
Mahadevan R., *Nature* **394**, 651 (1998)
Mannheim K., Schulte M. & Rachen J., *Astron. & Astrophys.*, **303**, L41 (1995)
Markoff S., Falcke H., & Fender R., *Astron. & Astrophys.* **372**, L25 (2001)
Mizuno Y., Nishikawa K.I., Koide S., Hardee P., Fishman G.J., Proceedings of the VI Microquasar Workshop: Microquasars and Beyond. September 18-22, 2006, Como, Italy., p.45.1, astro-ph/0609344
Moderski R., Sikora M., *Month. Not. Roy. Astr. Soc.* **283**, 854 (1996)
Nagar N. M., Falcke H., Wilson A. S. & Ho L. C., *Astrophys. J.* **542**, 186 (2000)
Nagar N. M., Wilson A. S. & Falcke H., *Astrophys. J.* **559**, L87 (2001)
Nagar N. M., Falcke H., Wilson A. S. & Ulvestad J. S., *Astron. & Astrophys.* **392**, 53 (2002)
Nagar N. M., Falcke H. & Wilson A. S., *Astron. & Astrophys.* **435**, 521 (2005)
Nitta S., Takahashi M. & Tomimatsu A., *Phys. Rev.* **D 44**, 2295 (1991)
Novikov I. D. & Thorne K. S., 1973 in Black Holes, ed. C. DeWitt & B. DeWitt (New York: Gordon & Breach) p. 343
Page D. N. & Thorne K. S., *Astrophys. J.*, **191**, 499 (1974)
Park S. J. & Vishniac E. T., *Astrophys. J.*, **332**, 135 (1988)
Perez-Fournon I. & Biermann P. L. *Astron. & Astroph* **130**, L13 (1984)
Shakura N. I., *Astronomicheskii Zhurnal* **49**, 921 (1972)
Shakura N. I. & Sunyaev R. A., *Astron. & Astroph* **24**, 33 (1973)
Shapiro S. L., Lightman A. P., Eardley D. M., *Astrophys.*

J. **204**, 187 (1976)
Shibata M. & Sasaki M., *Phys. Rev.* **D 58**, 104011 (1998)
Sikora M, Begelman M. C., Madejski G. M., Lasota J.-P., *Astrophys. J.*, **265**, 272 (2005)
Thorne K. S., *Astrophys. J.* **191**, 507 (1974)
Thorne K. S. & Price R. H. *Astrophys. J.* **195**, L101 (1975)
Thorne K. S., Price R. H. & Macdonald D. A. 1986 Black Holes: The Membrane Paradigm. (New Heaven: Yale Univ. Press)
Toomre A., Toomre, J *Astrophys. J.* **178**, 623 (1972)
Uzdensky D. A. *Astrophys. J.* **620**, 889 (2005)
Wang D. X., Xiao K. & Lei W. H., *Month. Not. Roy. Astr. Soc.* **335**, 655 (2002)
Wang D. X., Lei W. H. & Ma R. Y., *Month. Not. Roy. Astr. Soc.* **342**, 851 (2003)
Whysong D. & Antonucci R., *New Astronomy Reviews* **47**, 219 (2003)
Windhorst R. A., van Heerde G. M. & Katgert P., *Astron. Astrophys. Suppl. Ser.* **58**, 1 (1984)
Yuan F., Markoff S., & Falcke H., *Astron. Astrophys.* **383**, 854 (2002)
Yuan F., Markoff S., Falcke H., & Biermann P. L., *Astron. Astrophys.* **391**, 139 (2002)
Znajek R. L., *Month. Not. Roy. Astr. Soc.* **179**, 457 (1977)